Doctoral Thesis

The effects of acidic extracellular environments on TCR signal transduction

2013

Xin Wang

CONTENTS

GENERAL INTRODUCTION

In mammals, blood and tissues are usually maintained in a narrow range of pH around 7.4 mainly through regulation of respiration and renal acid extrusion. However, mammalian cells are often exposed to acidic environments in diseased areas such as inflammatory loci [1,2] and cancer nests [3]. Alterations in the microenvironments at the sites of infection and inflammation have been studied since the 1940s. The development of acidic environments is a hallmark of inflammatory processes and is attributed to the local increase of lactic-acid production by anaerobic glycolysis and to the presence of short-chain, fatty acid by-products of bacterial metabolism [4,5]. In solid tumors, the tumor microenvironments are also usually more acidic than normal, with values of extracellular pH ranging from 5.8 to 7.4, both in human and rodent malignant tissues [6-8].

Although immune cell infiltration is often observed in acidic inflammatory sites and tumor areas [9-12], relatively few studies have focused on the effect of extracellular acidic pH on the function of immune cells [13]. Observations made in stimulated macrophages indicated that extracellular acidification results in the inhibition of superoxide anion production, Fc-mediated phagocytosis, and TNF-α release [14], whereas Grabowski et al. [15] showed that environmental acidification increases the phagocytosis of opsonized particles by macrophages. Calcium ion mobilization, shape change response, up-regulation of CD18 expression, production of H_2O_2, and release of myeloperoxidase were markedly enhanced in neutrophils stimulated in acidic pH medium [16]. Müller et al. [17] showed impaired cytotoxic activity of natural killer (NK) as well as lymphokine-activated killer (LAK) cells at acidic pH. Exposure of murine dendritic cells (DCs) to pH 6.5 stimulates macropinocytosis and cross-presentation of extracellular antigens by MHC class I molecules [18]. Moreover, transient exposure to acidic conditions triggers not only the phenotypic maturation of human

DCs, but also a high level of IL-12 production [19]. The different signaling pathways have been investigated under different pH conditions in Jurkat T cells [20] and the phosphorylation levels of p38 and ERK were elevated at acidic pH [21]. These previous studies support the notion that acidic extracellular environments exert a great influence on immune response. However, it is still unclear how extracellular low pH affects TCR signaling.

Cellular signal transduction is initiated by the binding of a ligand to its receptor. The receptor generally functions in the complex form including homo- and hetero-multimers before and after the ligand binding [22-26]. Clustering of transmembrane proteins on the cell surface was proposed in the lipid raft model of the plasma membrane [27]. Cholestrol, unsaturated sphingolopids and lipid modified proteins etc do not distribute uniformly in the plasma membrane [28]. It is suggested that proteins may exist in “protein islands” connected to the cytoskeleton molecules (protein island model) [29]. Clustering of TCR complex is the first event for immune cell responses. The foreign antigens are recognized by T cell antigen receptor (TCR) on the cell surfaces, and the T cells were activated to initiate immune responses [30]. The membrane organization of TCR on the T cell surface has been investigated [31-33]. Similarly, linker of activated T cells (LAT) was also proposed to exist in “protein islands” on the surface of mast cells and T cells [34]. Microscopic techniques have shown the separate clusters of TCR and LAT in pre-activated T cells, and these clusters transiently concatenate into microclusters upon antigen recognition [35]. The costimulation of TCR with CD28 was reported to require co-localization of TCR and CD28 at the plasma membrane [36]. It is remain unclear why such complex formation is required for signal initiation and how the complex is formed. Woolf and Linderman [37] proposed that the self-assembly is induced by protein dimerization when the binding speed is higher than the diffusion rate of proteins.

In this study, I investigated how acidic extracellular environments affects TCR signaling and examined the model of cluster formation proposed by Woolf and Linderman with Monte Carlo simulation.

CHAPTER 1

How does the extracellular low pH affect TCR signaling ?

1-1. Introduction

T cells have a key role in immune response, and T cell signal transduction has been investigated since the mid-1980s. Following antigen presentation to TCR by APC (antigen-presenting cell), the binding of antigen/MHC complexes to the TCR triggers the tyrosine phosphorylation of the ITAMs (Immunoreceptor Tyrosine-based Activation Motifs), present in the TCR-associated CD3-ξ subunits. The activated ITAMs function by orchestrating the sequential activation of the Src-related PTKs (Protein Tyrosine Kinases): Lck and Fyn, which initiate TCR signaling, followed by the activation of ZAP-70 (tyrosine kinase-associated protein of 70 kDa) or the related Syk kinase, which further amplifies the response [38]. The translocation of Lck and ZAP-70 is regulated by RhoH (an hematopoietic-specific, GTPase-deficient Rho GTPase) [39]. The alternative TCR/CD3/FcRγ complex recruits and activates Syk, instead of ZAP-70 [40]. These various PTKs phosphorylate an adaptor protein LAT, ultimately resulting in the phosphorylation and activation of phospholipase C-γ (PLC-γ) [41]. PLC-γ cleaves phosphatidylinositol 4,5-bisphosphate (PIP2) in the plasma membrane to generate diacylglycerol, which activates protein kinase C (PKC) and Ras-dependent pathways, and 1,4,5-inositol trisphosphate (IP3), which causes entry of Ca^{2+} to cytosol from two sources: the endoplasmic reticulum (ER) and the extracellular fluid [42]. The increase in $[Ca^{2+}]_i$ consequently leads to the activation of signal proteins and transcription factors, including NFAT, NF-κB, and JNK1 [43-45]. In turn, these transcription factors regulate the expressions of several inducible genes such as IL-2, that mediate diverse genetic programs including immune effector functions, cell proliferation, cell differentiation, and cell death (Fig. 1-1).

In this study, I investigated the effect of extracellular acidic environments on TCR signal transduction in Jurkat T cell lines and human T cells from peripheral

blood. The activation of proteins in the initial complex and well-studied signal proteins in the middle of the pathways, the cytosolic level of free calcium ions as second messengers, and cytokine gene expression as a target of the TCR signaling were examined with cells cultured at acidic pH.

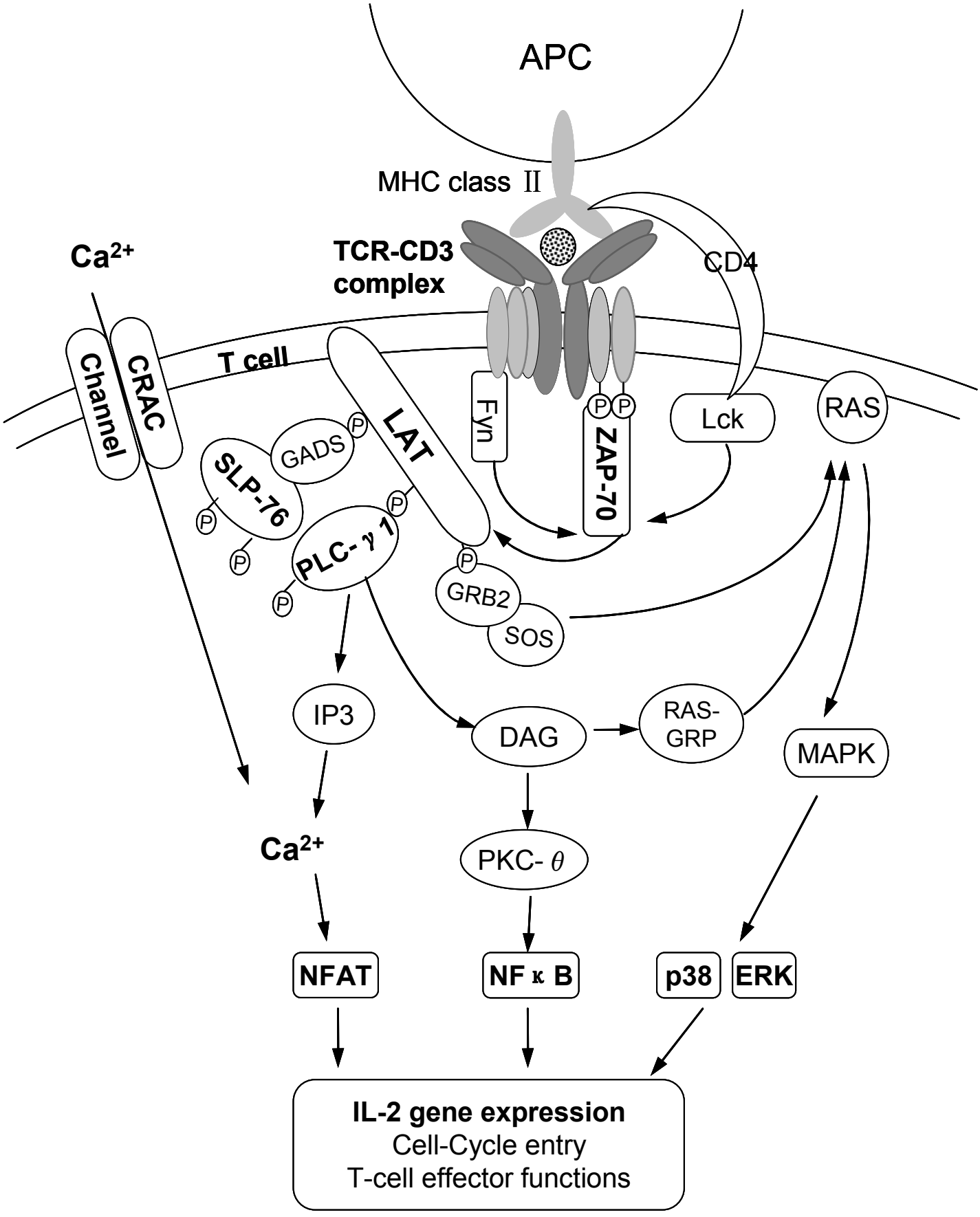

Fig. 1-1. Proximal signalling complexes and downstream responses induced by T-cell receptor (TCR) ligation.

1-2. Materials and Methods

Cells and antibodies

Human acute leukemia T cell line Jurkat E6.1 cells were supplied by Takashi Saito (RIKEN, Japan). Jurkat P116 cells were a gift from Shigeo Koyasu (Keio University, Japan) with the permission of Robert T. Abraham (The Burnham Institute, CA). Jurkat J14 and J.CaM2.5 cell lines were gifts from Arthur Weiss (California University, San Francisco). Anti-ZAP-70 monoclonal antibody (mAb), anti-phospho- -ZAP-70 (Y319) mAb, anti-Lck (Y505) mAb, anti-LAT (Y171) mAb, anti-ERK1 (MK12) mAb, anti-phospho-ERK1/2 (T202/Y204) mAb, Anti-NFAT-1 and anti-p38α (27/p38a/SAPK2a) mAb were obtained from BD Biosciences. Anti-phosphotyrosine mAb (4G10, Upstate Biotechnology), anti-phospho-CD3-ξ mAb (Y142, Epitomics), anti-glyceraldehyde 3-phosphate dehydrogenase (GAPDH) mAb (Cell Signaling), anti-phopho-p38 (T180/Y182, Sigma) mAb, anti-phospho-phospholipase C-γ1 (PLC-γ1) mAb (Y783, Cell Signaling), and anti-Syk antibody (Cell Signaling) were purchased. Anti-human CD3 mAb (OKT-3) and anti-human CD28 mAb (CD28.6) were purchased from eBioscience. Goat anti-mouse IgG conjugated with alkaline phosphatase (AP) and goat anti-rabbit IgG conjugated with AP antibodies were purchased from Sigma-Aldrich. Goat anti-rabbit IgG horseradish peroxidase (HRP)-linked antibody and goat anti-mouse IgG HRP-linked antibody were obtained from Cell Signaling.

Cell culture

Jurkat cell lines were cultured in RPMI-1640 (Wako Co., Japan) containing 10 μg/ml gentamicin and 5 μg/ml fungizone supplemented with 10% FBS at 37°C under 5% CO_2. For culture at different pH values, cells were transferred to RPMI-1640 containing 10 μg/ml gentamicin, 5 μg/ml fungizone, 10% FBS, and 10 mM PIPES [piperazine-N,N'-bis(2-ethanesulfonic acid)] for pH 6.3 or 10 mM HEPES [4-(2-hydroxyethyl) 1-piperazineethanesulfonic acid] for pH 7.6 instead of

Na_2CO_3, and cells were cultured without CO_2 gas supply. Medium containing FBS was often contaminated with germs when medium pH was adjusted, and it was hard to sterilize medium containing FBS. Therefore, medium pH was first adjusted to 6.2 and 7.7 by the addition of NaOH before the addition of FBS. After sterilization of the medium by filtration, FBS was added. After the addition of FBS, the pH values changed into 6.3 and 7.6, respectively.

Isolation of human T cells from peripheral blood

Human peripheral blood was obtained from a adult healthy volunteer. Peripheral blood mononuclear cells (PBMC) obtained from the healthy donor were isolated by density gradient centrifugation over Ficoll-Hypaque 1077 (Pharmacia, Uppsala, Sweden). PBMC were washed twice in ice-cold buffer (PBS, pH7.2, 0.5%BSA, 2 mM EDTA) and subsequently used for magnetic cell sorting. Untouched Pan T cells were purified by negative selection with human Pan T cell isolation Kit (Miltenyi Biotec, Germany) and BD IMagnet (BD Biosciences) according to the manufacturers' instructions. Purified cells were then cultured under pH 7.6 and pH 6.3 as described above for 24 h.

Western blot analysis

Cells were cultured under various pH conditions as described above for 24 h. Then anti-CD3 monoclonal antibodies (OKT-3) and/or anti-CD28 monoclonal antibodies (CD28.6) were added to the culture medium. After incubated for the indicated time, cells were harvested, washed with ice-cold PBS (10 mM sodium phosphate, pH 7.0, containing 137 mM NaCl, 4 mM KCl, 10 mM NaF and 1 mM Na_3VO_4), and collected by centrifugation. The resulting pellet was resuspended in lysis buffer (50 mM Tris–HCl, pH 7.8, 1% NP-40, 20 mM EDTA, 10 mM NaF, 1 mM Na_3VO_4, 1 mM phenylmethylsulfonyl fluoride, 1 μg/ml aprotinin and 0.2 μM leupeptin) and incubated for 20 min on ice. The suspension was centrifuged at 10,000 rpm for 10 min. NE-PER Nuclear and Cytoplasmic Extraction Kit (Thermo

Scientific) was used for cell lysis and extraction of separate cytoplasmic and nuclear protein fractions. The collected supernatants were mixed with 4×sodium dodecyl sulfate (SDS)-PAGE sample buffer (125 mM Tris–HCl, pH 6.8, 30% glycerol, 4% SDS, 10% β-mercaptoetanol and 0.05% bromophenol blue) and boiled for 90 seconds. The mixture was applied to a 10% polyacrylamide gel containing 0.1% SDS. Proteins separated by gel electrophoresis were transferred to a PVDF membrane. The membrane was blocked with 3% bovine serum albumin in PBS and then incubated with antibodies against target proteins, followed by AP or HRP conjugated anti-mouse IgG or anti-rabbit IgG. GAPDH in the cell extracts was used as a loading control.

Measurement of the concentration of cytosolic free calcium ions ($[Ca^{2+}]_i$)

After Jurkat cells had been cultured in pH 7.6 and pH 6.3 media for 24 h, cells were collected and washed with pH 7.6 and pH 6.3 culture media without phenol red, respectively.

(1) Measurement of $[Ca^{2+}]_i$ using fluorescence probe Fura-2. Cells (1.0×10^6 cells/ml) were incubated with 5 μM Fura-2-acetoxymethyl ester (Dojindo Co., Japan) for 45 min at 37°C in the same medium as that used for washing. Probenecid (2.5 mM) was added to the medium to avoid Fura-2 leakage. After Fura-2 loading, cells were washed and resuspended in the same medium. The fluorescence from the Fura-2-loaded cells was monitored with a ratiometric fluorescence spectrophotometer (HITACHI, F-2500). The excitation wavelengths were 340 and 380nm, and emission was measured at 510 nm. Then OKT-3 (0.2 μg/ml) and/or CD28.6 (5 μg/ml) were added to the cell suspension. After incubation at 37°C for 5 min, fluorescence was monitored again under the same conditions. The $[Ca^{2+}]_i$ was estimated as described by Grynkiewicz et al. [46] using the following formula:

$$[Ca^{2+}]_i = Kd[(R-Rmin)/(Rmax-R)]Fmin(380)/Fmax(380)$$

where R is the ratio of the fluorescence intensity at 340 nm to the intensity at 380 nm, and Rmax and Rmin are the fluorescence ratios at 340 nm to that at 380 nm obtained with the addition of 2 mM $CaCl_2$ plus 5 μM ionomycin and further addition of 5 mM EGTA, respectively. Kd represents the apparent dissociation constant of Fura-2, and 224 nM was used in the present study. Fmax(380) and Fmin(380) are the fluorescence intensities obtained with the addition of 2 mM $CaCl_2$ plus 5 μM ionomycin and further addition of 5 mM EGTA, respectively. BPT2 (Calbiochem) was used to inhibit Ca^{2+} release-activated Ca^{2+} channels in the plasma membrane.

(2) **Measurement of Ca^{2+} mobilization with fluorescence probe Fluo-4.** Cells (1.0×10^6 cells/ml) were incubated with 4 μM Fluo-4-acetoxymethyl ester (invitrogen, USA) for 30 min at 37°C in the same medium as that used for washing. Probenecid (2.5 mM) was added to the medium to avoid Fluo-4 leakage. After loading, cells were washed and resuspended in the same medium containing 2 mM $CaCl_2$. After incubation at 37°C for another 30 min, 200 μl cells were applied in a 96 well plate (Perkin-Elmer, OptiPlate-96 F). The changes of fluorescence from the Fluo-4-loaded cells were monitored with a microplate reader (Perkin-Elmer, 2030 ARVO χ) at 485 nm excitation and 535 nm emission. OKT-3 (0.2 μg/ml) and/or CD28.6 (5 μg/ml), ionomycin were added to the cell suspension automatically with dispensers.

Measurement of intracellular pH (pH_i)

The pH_i was measured by the pH-sensitive fluorescent probe 2',7'-bis-(2-car--boxyethyl)-5-(and-6)-carboxyfluorescein (BCECF). Cells were loaded with 5 μM of BCECF acetoxymethyl ester (Dojindo Co., Japan) for 30 min at 37°C in pH 7.6 or pH 6.3 RPMI-1640 media (without phenol red) as described above. The resulting cells were rinsed and resuspended in the same medium. To obtain the pH calibration curve, cells were incubated with 4 μM of K^+/H^+ ionophore nigericin in calibrating RPMI-1640 media containing 140 mM KCl at pH 6.3, 6.6, 6.9, 7.2 or

7.5. The fluorescence of BCECF was monitored in a ratiometric fluorescence spectrophotometer (HITACHI, F-2500). The excitation wavelengths were 500 and 450 nm. The emission wavelength was 530 nm.

Real-time quantitative PCR

Total RNA was isolated with the use of a TRI Reagent (Sigma-Aldrich), according to the manufacturer's instructions. Total RNA (2 μg) was reverse-transcribed using Reverse Transcriptase (TOYOBO) in a total volume of 20 μl containing the random primer for 18S rRNA or the polyT primer for targeted genes. Real-time quantitative PCR amplification was performed with an ABI PRISM 7000 Sequence Detection System (Applied Biosystem) using the FastStart Universal SYBR Green Master[Rox] (Roche Diagnostics) according to the manufacturer's instructions. The PCR reaction was carried out with a mixture containing 12.5 μl of Real-time PCR Master Mix, 7.5 μM of each sense and antisense primer, 25 ng of cDNA, and nuclease-free water in a total volume of 25 μl. The standard thermal profile for PCR amplification was 50°C for 2 min, 95°C for 10 min, and 40 cycles of 95°C for 15 seconds and 60°C for 60 seconds.

Statistical analysis

Student's t-test was utilized in this study.

1-3. Results

Phosphorylation of CD3 and ZAP-70 induced by CD3 stimulation at acidic pH

We first measured the phosphorylations of proteins in the initial step of TCR signaling, CD3-ζ, Lck, Syk, ZAP-70, and LAT, at acidic pH without CD3 stimulation. The phosphorylations of CD3-ζ and ZAP-70 were increased obviously at acidic pH, but the phosphorylations of other proteins were not. Therefore, the phosphorylations of CD3-ζ and ZAP-70 were further examined with the addition of

OKT-3, the stimulator of TCR signaling. The phosphorylation levels of these two proteins were measured at 0, 5, 10, 15, 30, and 60 min after treatment with OKT-3. The phosphorylations reached a maximal level at 5 min after the addition of OKT-3 at both pH 7.6 and 6.3 (data not shown).

CD3-ξ was phosphorylated upon the addition of 0.2 μg/ml OKT-3 at pH 7.6 and the phosphorylation level was somewhat increased when the concentration of OKT-3 was increased to 4 μg/ml (Fig. 1-2A). In contrast, the phosphorylation level of CD3-ξ was maximal at pH 6.3 when 0.2 μg/ml of OKT-3 was added, and the level was higher than that at pH 7.6 (Fig. 1-2A). This result was supported by repeated measurements using separate culture. It should be noted that the medium pH decreased from 7.6 to 7.4 after 24 h culture, while the change in medium pH was less than 0.1 pH units after 24 h culture in pH 6.3 medium.

The phosphorylation level of ZAP-70 without CD3 stimulation was reported to be higher at pH 6.3 than that at pH 7.6 [21]. The activation of ZAP-70 induced by CD3 stimulation was again higher at pH 6.3 than that at pH 7.6 at any concentration of OKT-3 tested (Fig. 1-2B). In this experiment, the bands of p-ZAP-70 were faint at pH 7.6. When higher amounts of proteins were applied to the gel, the denser bands of p-ZAP-70 were observed upon the addition of OKT-3 at pH 7.6, and the staining of the denser bands at pH 6.3 approached saturation under the same conditions. The similar result was also obtained by stronger exposure (data not shown). These results demonstrate that the TCR signaling induced by OKT-3 is more active at acidic pH.

Phosphorylation of PLC-γ1 at acidic pH

ZAP-70 associated with TCR/CD3 complex phosphorylates an adaptor protein LAT, resulting in the phosphorylation of PLC-γ [41]. We next measured the phosphorylation of PLC-γ1. The phosphorylation level of PLC-γ1 was maximal at 5 min after the addition of OKT-3 at both pH 7.6 and 6.3. The phosphorylation of PLC-γ1 was induced more strongly by OKT-3 at pH 6.3, compared with that at pH

7.6. The phosphorylation level was slightly increased by the costimulation with CD28.6 at pH 7.6, while the costimulation did not increase the phosphorylation level at pH 6.3 (Fig. 1-3).

Increase in $[Ca^{2+}]_i$ under acidic conditions

It has been reported that the stimulation of CD3 increases $[Ca^{2+}]_i$ via the activation of PLC-γ and that the level is further increased by the addition of CD28.6 under neutral conditions [47,48]. Our present data confirmed the previous results at pH 7.6 (Fig. 1-4). The level of $[Ca^{2+}]_i$ was increased by the addition of OKT-3 at pH 6.3 to a higher level than that upon the addition of OKT-3 plus CD28.6 at pH 7.6 (Fig. 1-4). Interestingly, further addition of CD28.6 decreased the level of $[Ca^{2+}]_i$ induced by CD3 stimulation at pH 6.3 (Fig. 1-4). These results suggest that Ca^{2+} mobilization is induced only by CD3 stimulation under acidic conditions and that the stimulation of CD28 attenuates the Ca^{2+} mobilization induced by CD3 stimulation.

The Ca^{2+} mobilization was strongly inhibited by BTP2, a potent inhibitor of Ca^{2+} release-activated Ca^{2+} channels in the plasma membrane [49], at pH 7.6, while the inhibition was weak at pH 6.3 (Fig. 1-5). The inhibition was not strengthened after incubation with BTP2 for 20 min at pH 6.3 (data not shown). These results indicate that the increment of $[Ca^{2+}]_i$ after TCR activation in acidic conditions in Jurkat T cells is mainly contributed to the Ca^{2+} entry through CRAC channel and Ca^{2+} can be mobilized from cytosolic organelles besides the extracellular fluid at acidic pH.

The Jurkat mutants, P116 (ZAP-70$^-$), J.CaM2.5 (LAT$^-$) and J14 (SLP-76$^-$), have less ability to increase $[Ca^{2+}]_i$ when CD3 is stimulated [50-52]. In agreement with these previous reports, the level of $[Ca^{2+}]_i$ upon addition of OKT-3 was lower in these mutants than that in the wild type at pH 7.6 (Fig. 1-6). The increments of $[Ca^{2+}]_i$ in P116 and J.CaM2.5 were also lower than that in the wild type at pH 6.3. In contrast, the increased level by the addition of OKT-3 in J14 was similar to that of the wild type at pH 6.3 (Fig. 1-6). These results imply that the increase in $[Ca^{2+}]_i$

is mediated through ZAP-70 and LAT, but not SLP-76 under acidic conditions.

A rapid increase in $[Ca^{2+}]_i$ is seen when resting T cells are treated anti-CD3 antibodies. This response in a minority of T cells occurs within 30 s of activation and has also been reported by June et al. [53]. The Ca^{2+} mobilization were determined by Fluo-4 with Jurkat and Jurkat mutant cells after CD3 and/or CD28 stimulation in a real time manner. And the results were consistent with those obtained with Fura-2 that Ca^{2+} mobilization was more strongly induced by CD3 stimulation under acidic conditions through ZAP-70 and LAT, but not SLP-76. And the costimulation of CD28 attenuated the Ca^{2+} mobilization induced by CD3 stimulation (Fig. 1-7).

Cytosolic pH (pH_i) at acidic pH

There are two possible explanations for the high activation of TCR signalling at acidic pH. One is that the activation upon the binding of antibodies to TCR is affected by the external pH. The second one is that the phosphorylation activity is dependent on the cytosolic pH. The pH_i values were 7.31 ± 0.05 (n = 6) and 6.70 ± 0.05 (n = 6) in pH 7.6 and 6.3 media, respectively. The pH_i values after the addition of 0.2 μg/ml of OKT-3 were 7.32 ± 0.06 (n = 6) and 6.66 ± 0.05 (n = 6) in pH 7.6 and 6.3 media, respectively, indicating that CD3 stimulation has no significant effect on the pH_i regulation. Taken together with results shown in Fig. 1-2 that the induction of TCR signalling was higher at acidic pH at any concentration of OKT-3 tested, the second explanation may be more possible.

Activation of ERK and p38 at acidic pH

MAPK p38 and ERK are phosphorylated downstream of TCR signalling [54,55]. The phosphorylation levels of MAPK p38 and ERK without CD3 stimulation were found to be higher at pH 6.3 than those at alkaline pH [19,21]. In the present study, the activation of MAPK p38 and ERK induced by CD3 stimulation was examined. The phosphorylation level of ERK was maximal at 5 min after the addition of

OKT-3 at both pH 7.6 and 6.3 (data not shown). The phosphorylation of ERK1/2 was stimulated by the addition of OKT-3 both at pH 7.6 and 6.3, and the activation level increased as pH decreased (Fig. 1-8A). No activation of ERK2 in the presence of OKT-3 was observed in P116 cells at pH 6.3, whereas the phosphorylation of ERK1 was stimulated slightly by the addition of OKT-3 under the same conditions (Fig. 1-8A). The bands of p-ERK2 were faint, especially in the presence of OKT-3, at pH 7.6 (Fig.1-8A), compared with the data reported previously [54,55]. When higher amounts of proteins were applied to the gel, the denser bands of p-ERK2 were observed at pH 7.6, and the staining approached saturation at pH 6.3 (data not shown).

The phosphorylation level of p38 was maximal at 30 min after the addition of OKT-3 at both pH 7.6 and 6.3. The activation of p38 was observed without the addition of OKT-3 at pH 6.3, and was increased slightly after CD3 stimulation (Fig. 1-8B). No p38 activation was observed in the P116 cells at pH 7.6 or 6.3 regardless of the presence or absence of OKT-3. These results suggest that the TCR signaling pathway that activates ERK1/2 and p38 is also dependent on ZAP-70 and is more active at acidic pH.

Nuclear translocation of NFAT and NFκB at acidic pH

Calcium signaling activates the phosphatase calcineurin and induces movement of the transcription factor NFAT proteins into the nucleus [56]. The dephosphorylation and translocation of NFAT was examined and found that under acidic condition, the nuclear translocation of NFAT induced by CD3 was much weaker than that at pH 7.6 (Fig. 1-9）. Ca^{2+}-dependent phosphatase calcineurin synergized with PKC-dependent pathways to degrade IκBα and result in the activation of NFκB [57]. To detect the effects of acidic conditions on the activation of NFκB pathway, I analyzed the nuclear translocation of transcription factor NFκB and the result showed that the movement of NFκB proteins into the nucleus was more strongely induced under acidic condition (Fig. 1-9).

Expressions of cytokines at acidic pH

Since CD3 stimulation was reported to induce cytokine production [58,59], we measured the expressions of cytokines under acidic conditions. The level of mRNA has been generally normalized using the mRNA level of β-actin or GAPDH. There are no data to show that the mRNA levels of these control genes are not affected by pH. We therefore measured the levels of 18S rRNA and mRNAs of β-actin and GAPDH. The levels of 18S rRNA and GAPDH mRNA were affected by neither pH nor OKT-3, while the mRNA level of β-actin was decreased at acidic pH. It should be noted that the same amount of RNA prepared from cells was used for all experiments. It has been reported that the content of ribosomes per cell was approximately 4×10^6[60], and the amount of GAPDH mRNA per cell can be estimated to be 8×10^5 copies using 18S rRNA as a control RNA.

The mRNA level of IL-10 calculated was higher than that of GAPDH, but the expression was dependent on neither OKT-3 nor pH (Fig. 1-10A). The mRNA level of IL-10 was almost the same in the wild type Jurkat, J.CaM2.5, and J14 cells at both pH 7.6 and 6.3 (data not shown), suggesting that the expression of the anti-inflammatory cytokine, IL-10, is independent of TCR signaling.

The expression of IL-2 was stimulated by OKT-3 and further increased by the costimulation with anti-CD28 at pH7.6 (Fig. 1-10B), in agreement with previous reports [58,59]. In contrast, the expression of IL-2 was not increased significantly by the addition of OKT-3 at pH 6.3, and the costimulation with anti-CD28 had no effect on the expression (Fig. 1-10B). These results suggested that IL-2 expression was independent from TCR signaling in Jurkat cells under acidic conditions. Furthermore, the mRNA level of IL-2 was less than 0.02% of ribosomal RNA and less than 0.1% of GAPDH mRNA. The similar results were obtained in cells treated with OKT-3 for 30 or 60 min. Under these circumstances, the binding chance of IL-2 mRNA to ribosomes seems to be very low. Furthermore, it can be argued that any regulator has a low binding affinity to target even if it is inactive. This means that expression of any gene always occurs at a low level without the

activation. Therefore, gene expression at a low level such as that of IL-2 observed at pH 6.3 might be insufficient to synthesize enough amounts for its function. Besides the relative changes examined generally to date, the absolute value of the mRNA level may be important in the investigation of gene expression.

It was reported that the expressions of IL-5 and INF-γ were dependent on $[Ca^{2+}]_i$ [49]. The mRNA levels of these two genes were less than 0.02% of the level of GAPDH mRNA and were independent of CD3 stimulation for 5, 30 and 60 min at pH 6.3 (data not shown). In addition to these genes, no significant increase in the expressions of IL-3, IL-4, IL-6, IL-9, IL-13, IL-16, IL-18, and TNF-α by CD3 stimulation was observed at pH 6.3 (data not shown). It remains unclear which gene is induced by CD3 stimulation at acidic pH.

The effects of acidic pH on TCR signaling in human peripheral blood T cells

I finally investigated the effect of extracellular acidic environments on TCR signal transduction in human T cells from peripheral blood. The activation of proteins in the initial signal complex - CD3-ζ, ZAP-70, LAT and the well-studied signal protein in the middle of the pathways- PLC-γ1, as well as Ca^{2+} mobilization, were examined with cells cultured at acidic pH. The phosphorylations of CD3-ζ, ZAP-70 and PLC-γ1 were induced by CD3 stimulation at pH6.3, but the levels were weaker than those at pH 7.6 (Fig. 1-11). The activation of LAT could not be induced upon the addition of OKT-3 regardless of pH change (data not shown).

The Ca^{2+} mobilization was induced by the addition of OKT-3 at pH 7.6, while no increment of $[Ca^{2+}]_i$ was observed at pH 6.3 (Fig. 1-12A). Although further addition of CD28.6 increased the level of $[Ca^{2+}]_i$ induced by OKT-3 at pH 6.3, the level was lower than that at pH 7.6 (Fig. 1-12B). These data indicate that the activation of TCR signaling induced by CD3 stimulation is impaired at acidic pH in human peripheral blood T cells.

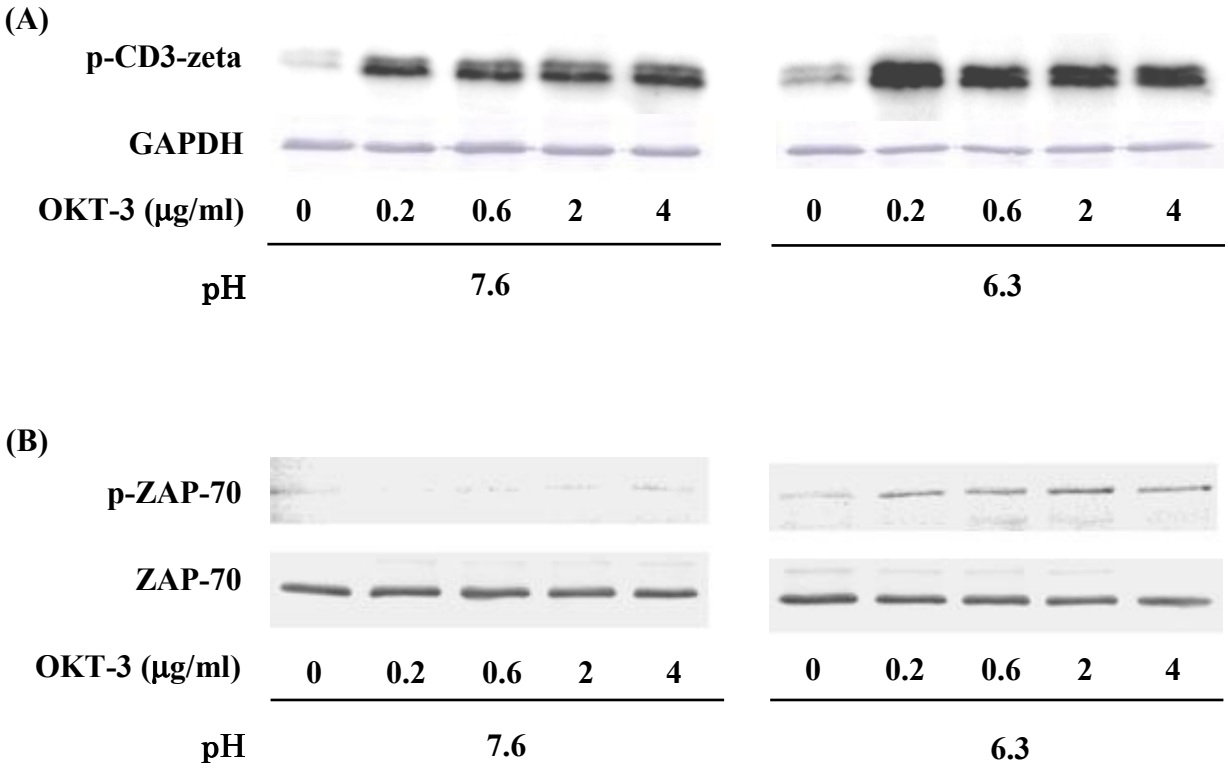

Figure 1-2. Phosphorylation of CD3- ξ and ZAP-70 in Jurkat T cells stimulated by OKT-3.

After Jurkat cells had been cultured in pH 7.6 or 6.3 media for 24 h, OKT-3 was added to the culture media at the indicated concentrations. After 5 min incubation with OKT-3 (0.2 μg/ml), the cells were harvested and whole cell extracts were analyzed using anti-p-CD3- ξ mAb, anti-ZAP-70 mAb, anti-p-ZAP-70 mAb, and anti-GAPDH mAb as described in Materials and Methods. (A) phosphorylation of CD3- ξ . (B) phosphorylation of ZAP-70.

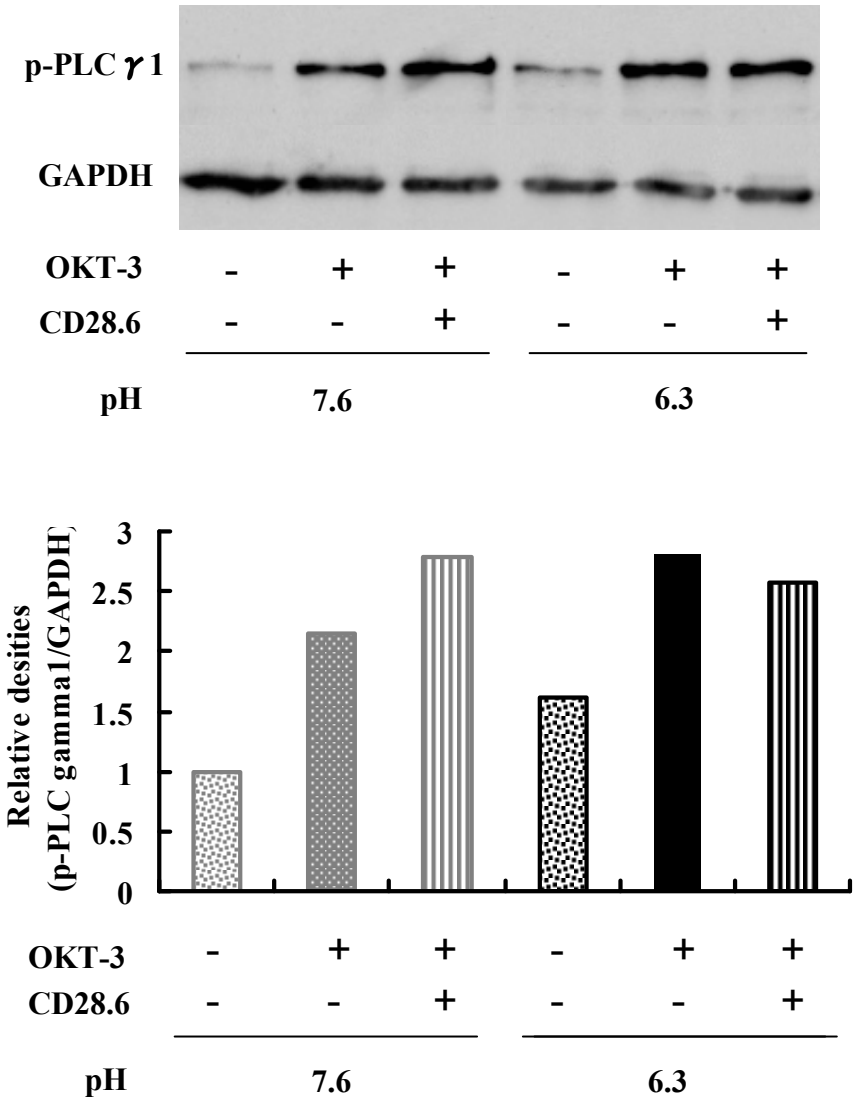

Figure 1-3. Phosphorylation of PLC-γ1 stimulated by OKT-3 and CD28.6 in Jurkat T cells.

After Jurkat cells had been cultured in pH 7.6 and 6.3 media for 24 h, they were stimulated with OKT-3 (0.2 μg/ml) and CD28.6 (5 μg/ml) for 5 min. Whole cell extracts were analyzed using anti-p-PLC-γ1 mAb and anti-GAPDH mAb as described in the legend of Figure 1-2.

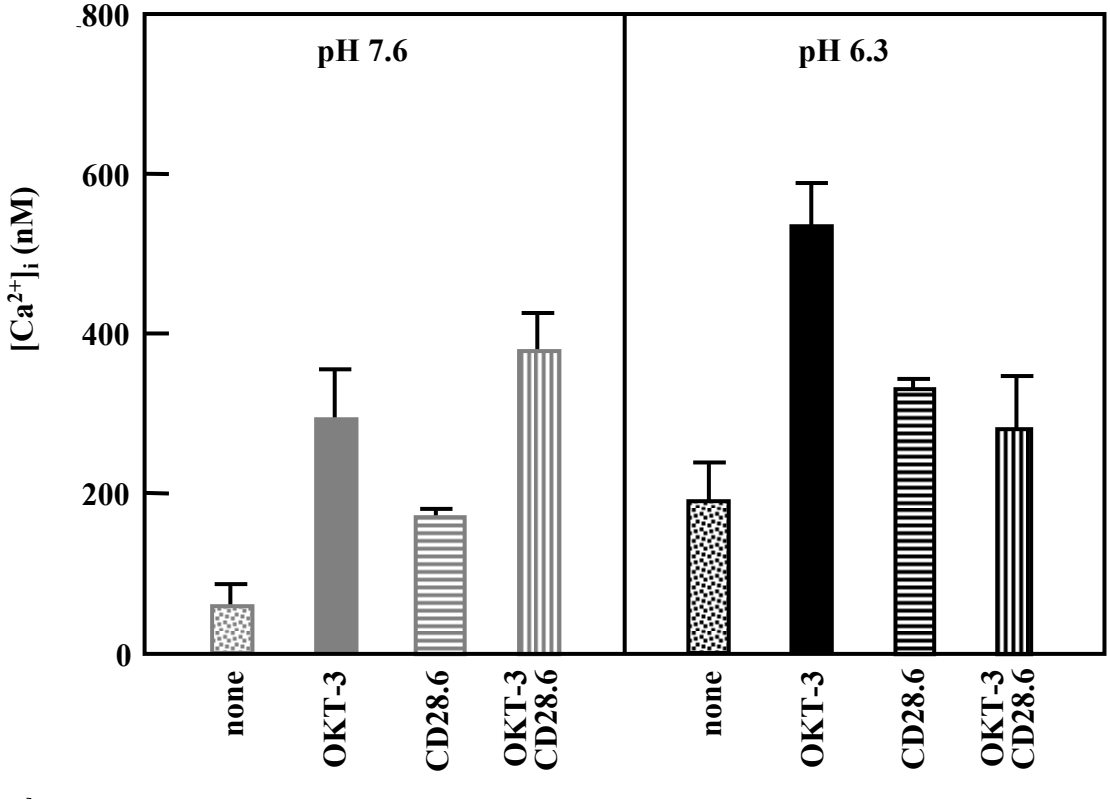

Figure 1-4. $[Ca^{2+}]_i$ in Jurkat cells stimulated by OKT-3 and CD28.6.
After Jurkat cells had been cultured in pH 7.6 and 6.3 media for 24 h, $[Ca^{2+}]_i$ was measured as described in Materials and Methods. The means and standard deviations of three measurements obtained from cells cultured independently are represented. p values of all combinations were less than 0.001 at pH 7.6 and 6.3.

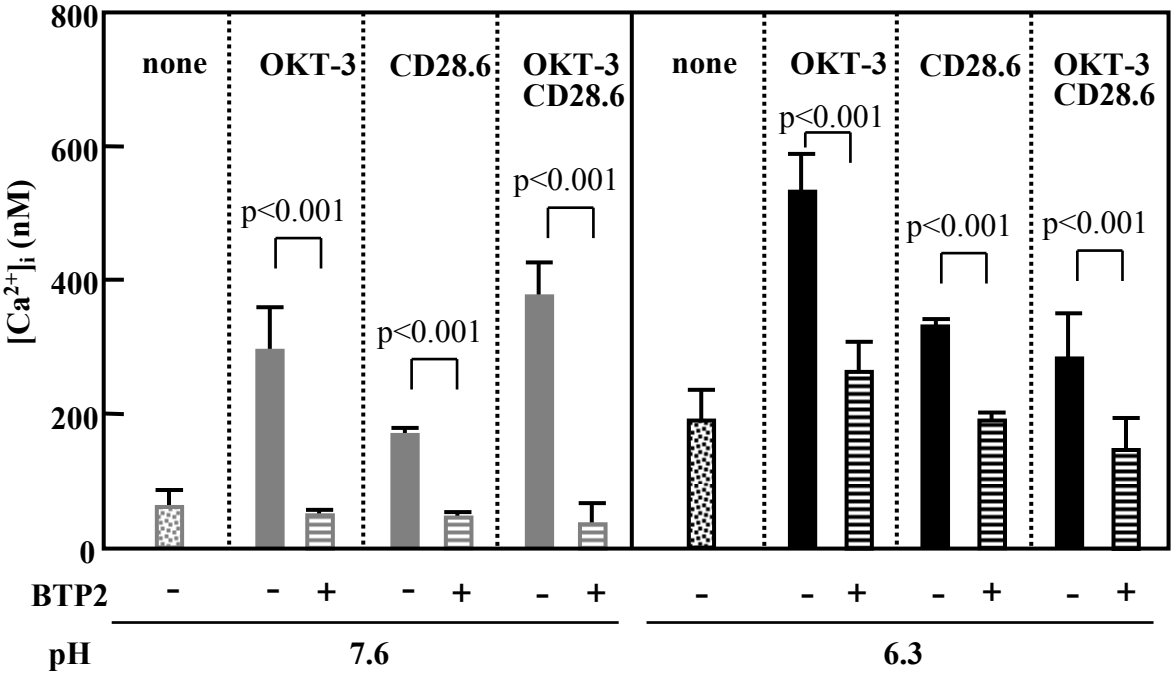

Figure 1-5. Effect of BTP2 on $[Ca^{2+}]_i$ in Jurkat cells stimulated by OKT-3 and CD28.6.

After Jurkat cells had been cultured in pH 7.6 and 6.3 media for 24 h, they were treated with BTP2 (10 μM) for 10 min and then stimulated with OKT-3 (0.2 μg/ml) and CD28.6 (5 μg/ml) for 5 min. $[Ca^{2+}]_i$ was measured as described in Materials and Methods. The means and standard deviations of three measurements obtained from cells cultured independently are represented. p values of statistical analysis are represented.

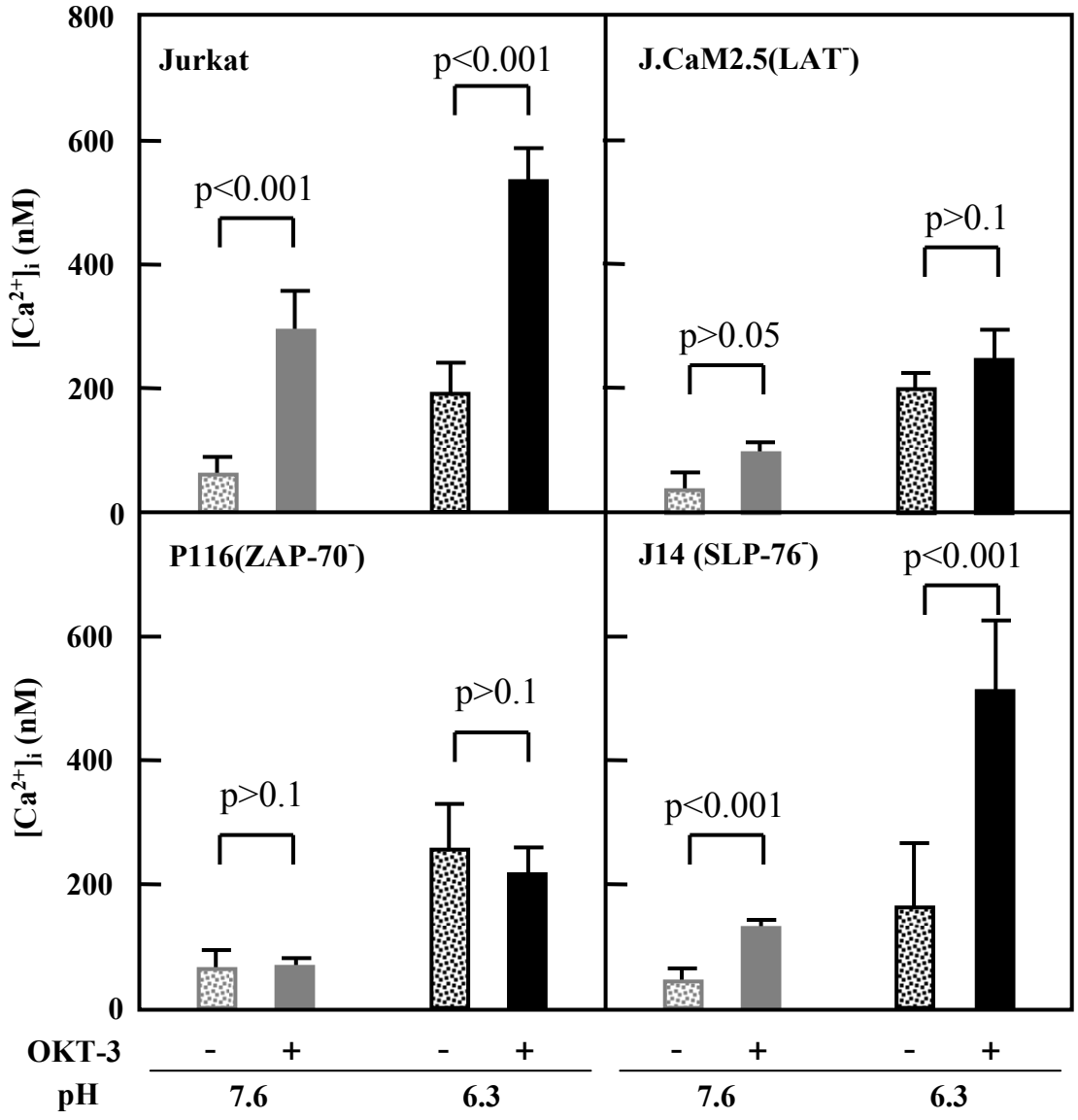

Figure 1-6. $[Ca^{2+}]_i$ in Jurkat mutant cells stimulated by OKT-3.
After the Jurkat mutant cells indicated had been cultured in pH 7.6 and 6.3 media for 24 h, $[Ca^{2+}]_i$ was measured as described in Materials and Methods. The means and standard deviations of three measurements obtained from cells cultured independently are represented. p values of statistical analysis are represented.

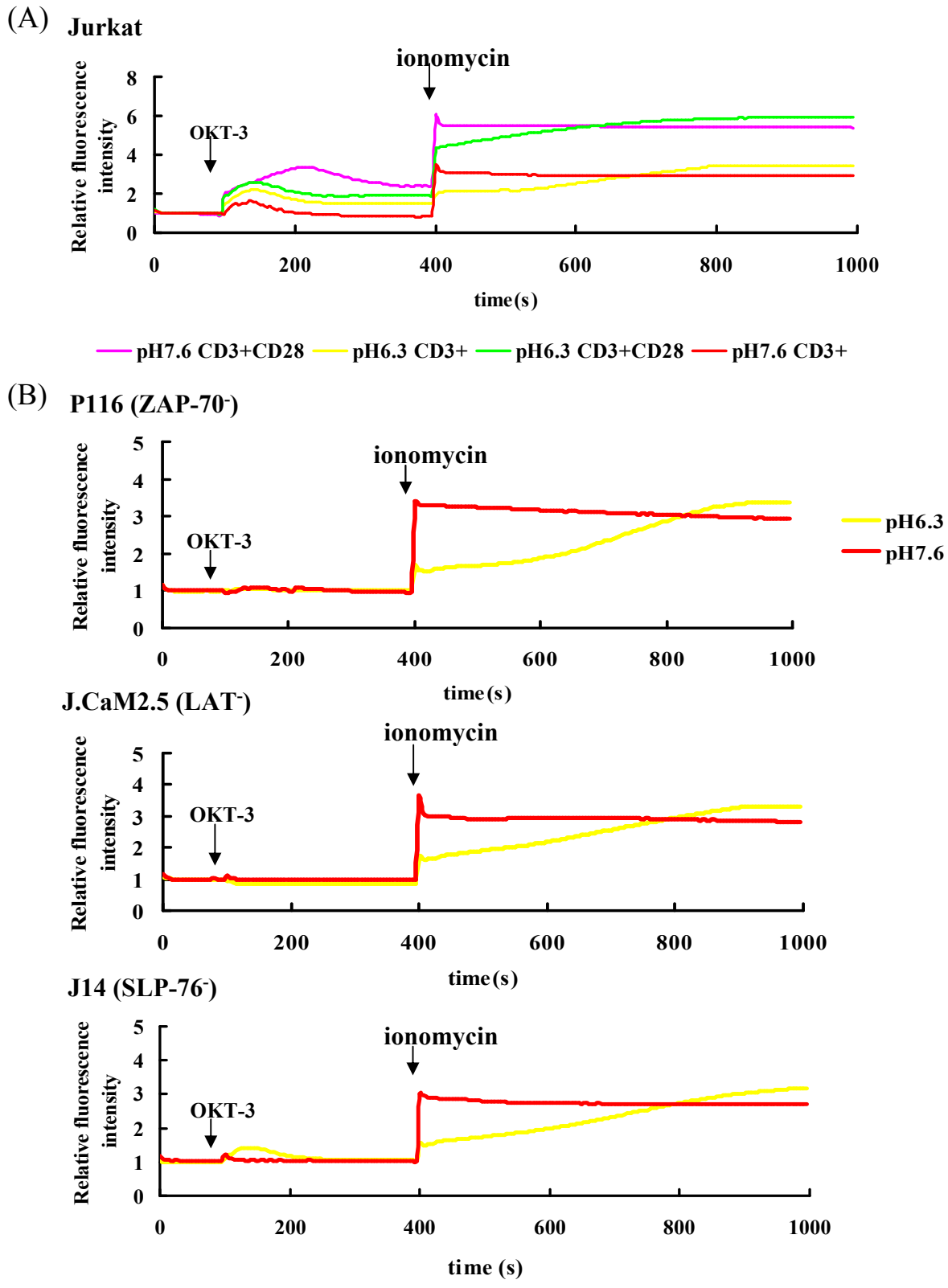

Figure 1-7. Ca^{2+} mobolization in Jurkat and Jurkat mutant cells stimulated by OKT-3 and CD28.6.

After cells indicated had been cultured in pH 7.6 and 6.3 media for 24 h, $[Ca^{2+}]_i$ was measured as described in Materials and Methods. (A) Ca^{2+} mobolizaion in Jurkat cells stimulated by OKT-3 and CD28. (B) Ca^{2+} mobolization in Jurkat mutant cells stimulated by OKT-3.

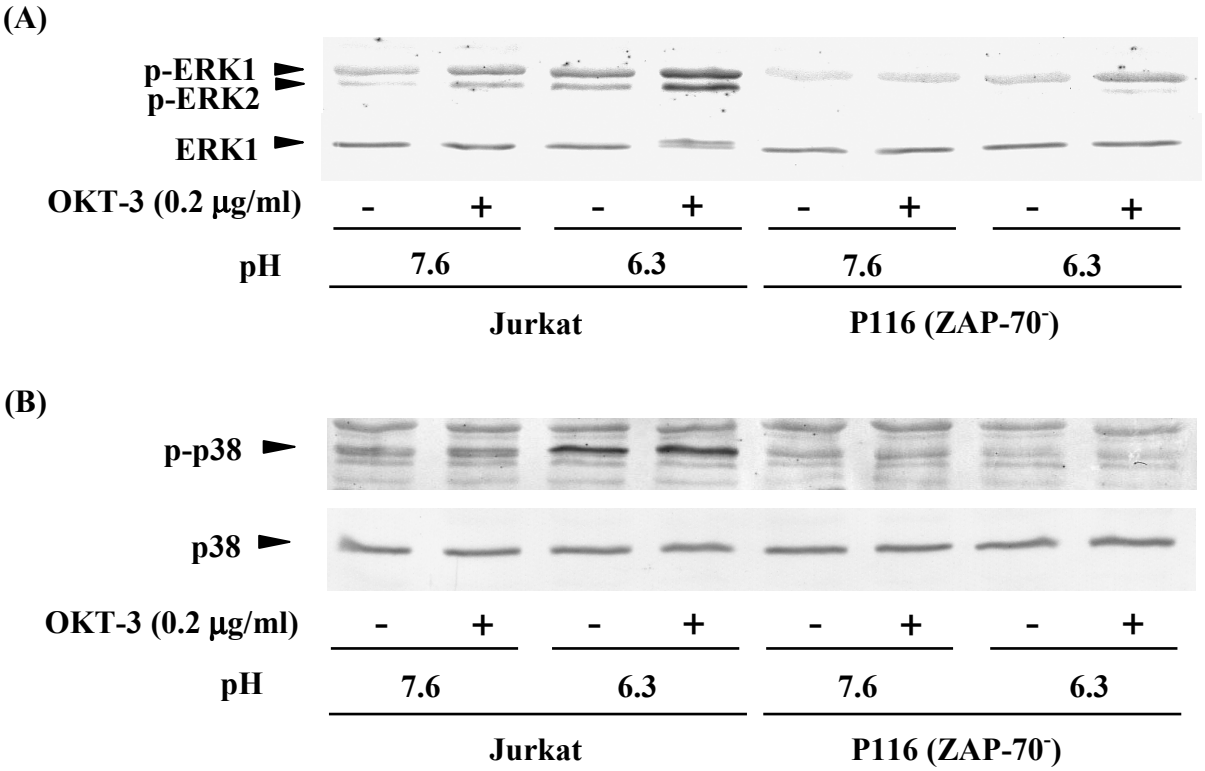

Figure 1-8. Phosphorylation of ERK and p38 upon the addition of OKT-3 in Jurkat and P116 cells.

Jurkat and P116 (ZAP-70$^-$) cells cultured in pH 7.6 and 6.3 media for 24 h were treated with or without OKT-3 (0.2 μg/ml) for 5 min (A) or 30 min (B). Whole cell extracts were analyzed using anti-p-ERK1/2 mAb, anti-ERK1 mAb, anti-p-p38 mAb, and anti-p38 mAb as described in the legend of Figure 1-2.

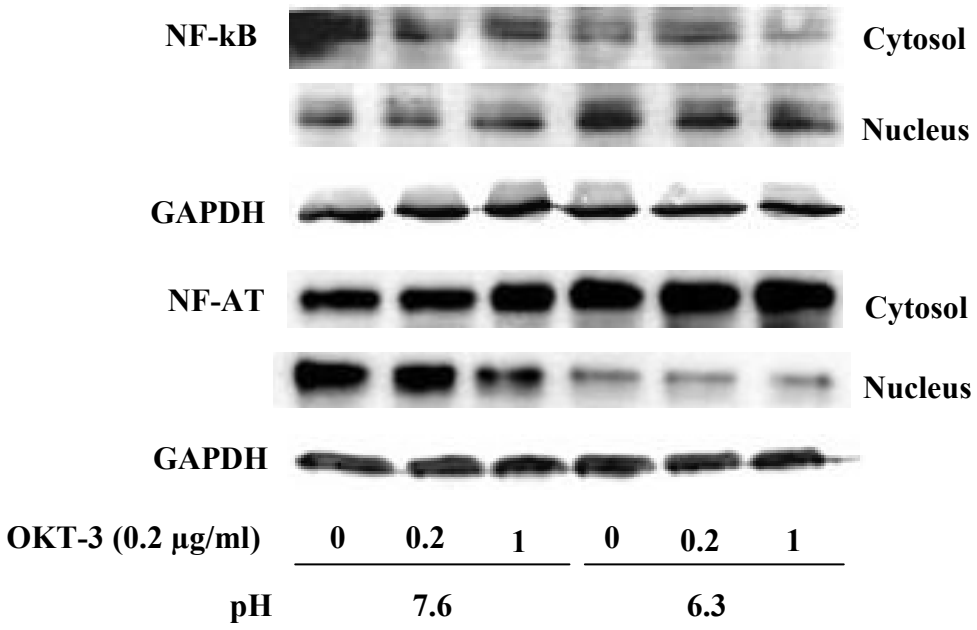

Figure 1-9. The nuclear translocation of transcription factors NF-κB and NFAT upon the addition of OKT-3 in Jurkat T cells.

Jurkat cells cultured in pH 7.6 and 6.3 media for 24 h were treated with the indicated concentration of OKT-3 for 4 hr. Cytosol and nuclear fractions were isolated by NE-PER Reagents. The proteins were analyzed by immunoblot using anti-NFκB mAb and anti-NFAT mAb.

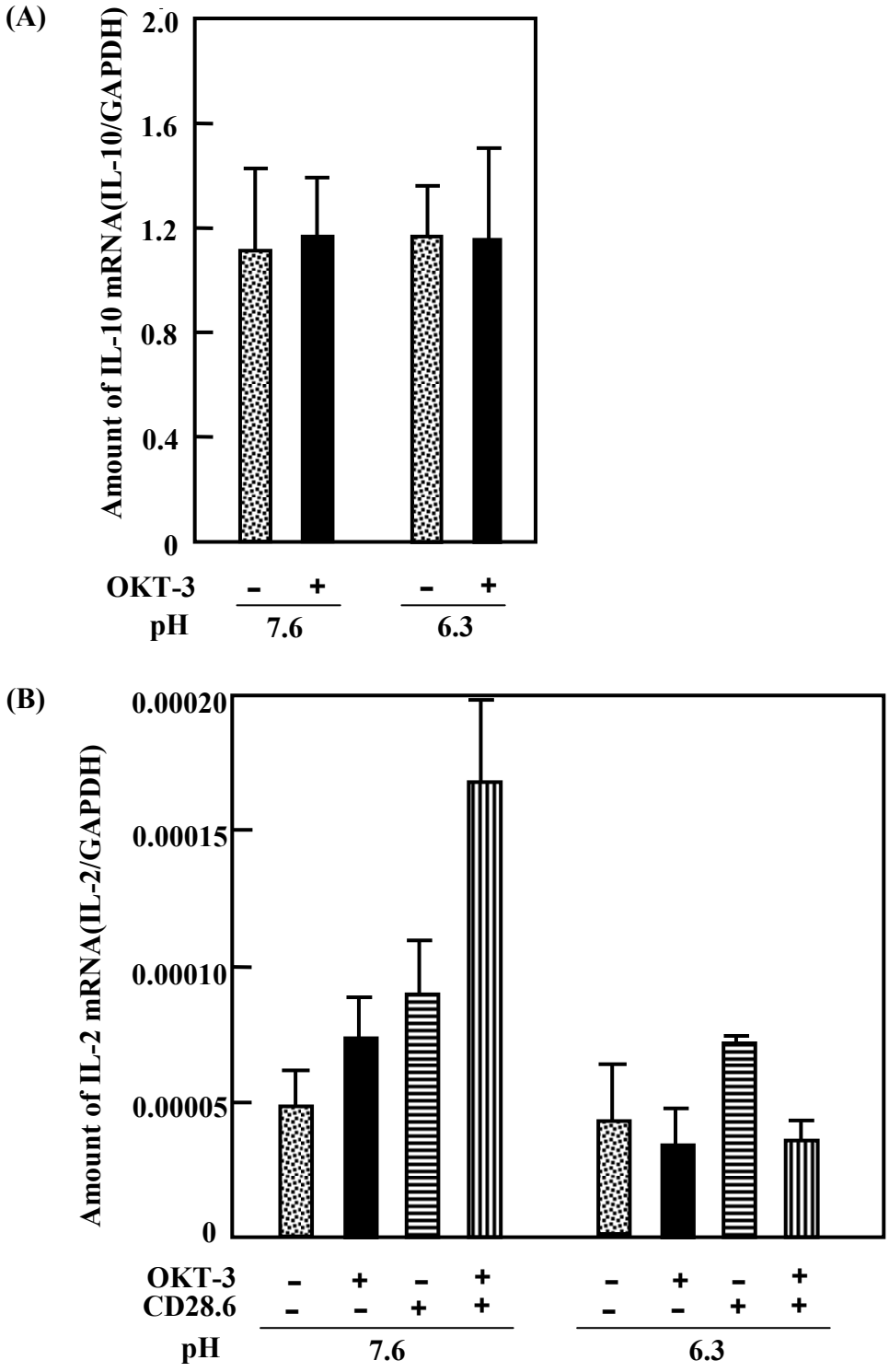

Figure 1-10. Expression of IL-10 and IL-2 in Jurkat cells.
Jurkat cells cultured in pH 7.6 and 6.3 media for 24 h were treated with OKT-3 (0.2 μg/ml) or CD28.6 (5 μg/ml) for 5 min. Whole RNA was extracted and mRNA levels of IL-10 (A) and IL-2 (B) were measured with real-time PCR as described in Materials and Methods. The means and standard deviations of six measurements obtained from cells of two independent cultures are represented. Statistical analysis of IL-2 expression: $p<0.01$ compared with no addition at pH 7.6; $p>0.3$ compared with "no addition" at pH 6.3.

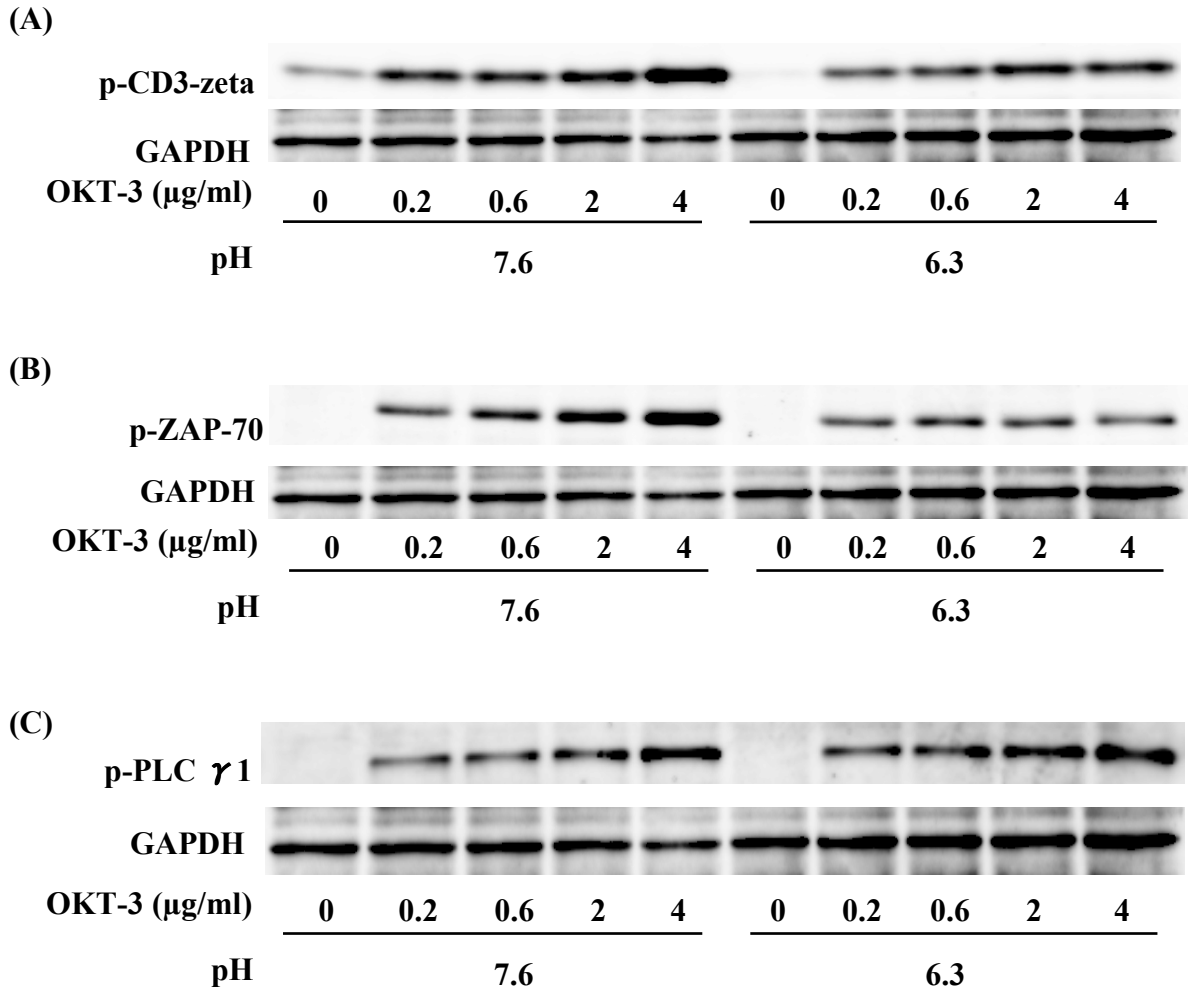

Figure 1-11. Phosphorylation of CD3-ξ, ZAP-70 and PLC γ1 in human peripheral blood T cells stimulated by OKT-3.

After human T cells from peripheral blood had been cultured in pH 7.6 or 6.3 media for 24 h, OKT-3 was added to the culture media at the indicated concentrations. After 5 min incubation with OKT-3 (0.2 μg/ml), the cells were harvested and whole cell extracts were analyzed using anti-p-CD3-ξ mAb, anti-p-ZAP-70 mAb, anti-p-PLC γ1 mAb and anti-GAPDH mAb as described in Materials and Methods. (A) phosphorylation of CD3-ξ. (B) phosphorylation of ZAP-70. (C) phosphorylation of PLC γ1

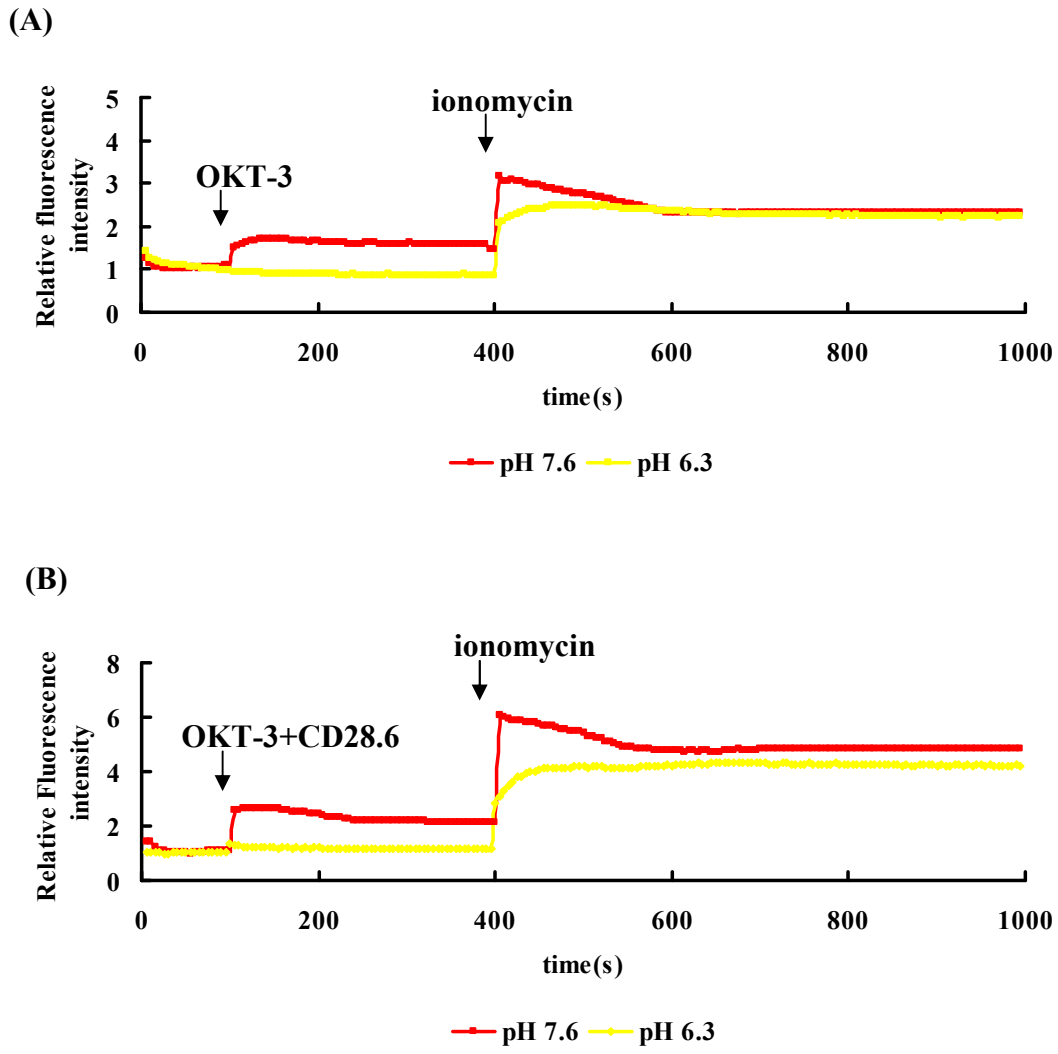

Figure 1-12. Ca^{2+} mobilization in human peripheral blood T cells stimulated by OKT-3 and CD28.6.

After cells had been cultured in pH 7.6 and 6.3 media for 24 h, Ca^{2+} mobilization was measured with Fluo-4 as described in Materials and Methods. (A) Ca^{2+} mobilization stimulated by OKT-3. (B) Ca^{2+} mobilization stimulated by OKT-3 and CD28.6.

1-4. Discussion

Immune cells migrate into diseased areas, such as inflammatory areas and cancer nests, to rehabilitate damaged tissues in such areas. Since inflammatory areas and cancer nests are acidic, investigations of immune cell functions under acidic conditions should prove useful for understanding the immune responses in vivo.

In the present study, the activation of proteins in the initial complex, CD3-ζ , LAT, Lck, Syk, and ZAP-70, phosphorylation of signal proteins in the middle of the pathways, PLC-γ, ERK, and p38, mobilization of calcium ions as second messengers, and cytokine gene expression as a target of the TCR signaling were examined with cells cultured at acidic pH. The TCR signaling was found to be more active under acidic conditions. The underlying mechanism remains unclear. One possibility is that the density of TCR on the cell surface is high at acidic pH. The TCR signaling was strongly activated by OKT-3 immediately after cells had been transferred to acidic medium (data not shown), suggesting that this possibility was less likely. The phosphorylation level of CD3-ξ was not markedly increased by the addition of OKT-3 at the concentrations more than 0.2 μg/ml (Fig. 1-2A), suggesting that the binding of OKT-3 to TCR was saturated at 0.2 μg/ml. Based on these results, it can be argued that the strong activation of TCR signaling is due to the rapid phosphorylation of signal proteins at the initial step but not the elevated complex formation of TCR with antibodies. The investigation of signal pathways has been carried out generally with cells incubated in serum free medium. Since pHi was decreased during serum starvation, serum starvation was not appropriate for the present study, and hence medium containing FBS was always used to avoid serum starvation. The phosphorylation levels of signal proteins we measured and the level of $[Ca^{2+}]_i$ were always high at acidic pH without the addition of OKT-3 (Fig. 1-2, 1-3, 1-8). The basal levels of activation varied with different lots of FBS. Therefore, the calcium ion mobilization may be induced partially by the contaminating antibodies in FBS even if OKT-3 is not added. The level of $[Ca^{2+}]_i$ upon the addition of OKT-3, rather than the change in $[Ca^{2+}]_i$ induced by the

addition of OKT-3, may be significant physiologically because the activation of the downstream steps is dependent on the level of $[Ca^{2+}]_i$ but not on its change.

In the present study, Ca^{2+} mobilization was more strongly induced under acidic conditions (Fig. 1-4, 1-6) while the activation of transcription factor NFAT and the expression of IL-2 was not induced (Fig. 1-9, 1-10). It was reported that the expressions of IL-5 and INF-γ were dependent on $[Ca^{2+}]_i$ [49]. The expression of these two genes could not be induced neither under acidic conditions. These results lead us to concern that the Ca^{2+}/NFAT pathway may play an important role in regulating cytokine expression in acidic environments. Further investigation of the transcriptional activity of NFAT under acidic conditions may be indispensable for our understanding of the immune response functioning at low pH conditions.

The deficiency in SLP-76 attenuated the calcium ion mobilization induced by CD3 stimulation at pH 7.6 as reported previously [61]. In contrast, the increase in $[Ca^{2+}]_i$ in the mutant deficient in SLP-76 was similar to that in the wild type at pH 6.3. Interestingly, the activation of PLC-γ1 and the calcium ion mobilization induced by CD3 stimulation were not increased by the costimulation with CD28 at acidic pH. Both were enhanced by the costimulation at pH 7.6 in agreement with previous reports [58,59]. These results imply that the TCR signaling pathway to mobilize calcium ions is different under acidic conditions.

It was reported that the costimulation of CD28 with TCR requires colocalization of TCR and CD28 at the plasma membrane [62]. TCR and CD28 might localize separately at acidic pH. Alternative explanation may be that the antibody binding to CD28 attenuates the binding of anti-CD3 antibody at acidic pH via the structural alteration of the CD3-CD28 complex, so that induces impaired interaction of downstream signal proteins such as Vav1 and Itk with PLC-γ1 [63], resulting in the attenuation of PLC-γ1 activation and Ca^{2+} mobilization.

Costimulation of TCR with CD28 protected against anergy induction [61], and CD28 costimulation led to a dramatic up-regulation in IL-2 expression [64,65]. CD28 was shown to play a key role on the generation of Th2 responses [66]. Our data showed that the CD28 stimulation further increased neither calcium ion

mobilization nor the IL-2 expression induced by TCR stimulation at acidic pH in Jurkat T cells (Fig. 1-4, 1-10). And the activation of TCR signaling induced by CD3 stimulation is impaired at acidic pH in human T cells from peripheral blood (Fig. 1-11, 1-12). These data lead us to argue that anergy induction is not repressed and immune response declines under acidic conditions. However, it should be noted that human peripheral blood T cells are a mixture of many kinds of T cells. Detailed purification should be performed in order to clarify the effects of acidic conditions on T cell functions. And immune cells have to rehabilitate damaged tissues in acidic diseased areas. Immune cell functions under acidic conditions may be different from that observed previously at alkaline pH. Further investigation under acidic conditions is indispensable for our understanding concerning immune responses, such as anergy and autoimmune, in acidic diseased areas. Since statins showed low cytotoxicity against cancer cells in alkaline medium used generally, these drugs were not developed as an anticancer medicine. Recently, clinical investigations have suggested that statins repress cancer progress in cancer patients. Our group found that statins had high cytotoxicity against cancer cells under acidic conditions [67]. Similarly, the screening of compounds in acidic medium may promote the development of new medicines for immunotherapy against cancer and inflammation.

CHAPTER 2

Do membrane proteins cluster without binding between molecules ?

2-1. Introduction

It is hard to examine the clustering of membrane protein complex experimentally because we have few useful methods to manipulate the complex formation without affecting the functions of the consisting proteins. One method to facilitate such examination would be kinetic analysis with the aid of the computer. Two types of computer simulation techniques are now available: numerical integration of differential equations and Monte Carlo simulation. The former method can address average behavior involving a large number of molecules and stochastic variations. In contrast, the latter can simulate both population behavior and single molecule dynamics. Monte Carlo simulation can also evaluate time-dependent fluctuations involving noise as well as cell-to-cell population heterogeneity [68].

Since one cell contains less than 100,000 molecules of a given membrane protein and there are variations in biological phenomena, the latter method may be more appropriate. Receptor-ligand formation and clustering of membrane proteins have already been simulated with Monte Carlo techniques [68-72], and their results revealed the usefulness of this technique for clarification of biological phenomena.

Various physiological meanings of the clustering of membrane proteins have been proposed [73-78], but the mechanism for this cluster formation remain unclear, although a few mechanisms have been proposed [37, 69, 79]. Woolf and Linderman [37] proposed that the self-assembly is induced by protein dimerization when the binding speed is higher than the diffusion rate of proteins. In this study, we found that different algorithms for Monte Carlo simulation gave different results concerning the cluster formation. The self-organization proposed by Woolf

and Linderman was seen in some algorithms, while cluster formation independent of the rate of the dimerization was simulated in other algorithms. We discussed which algorithm was more appropriate for the simulation of complex formation of membrane proteins, and concluded that the self-assembly is unlikely *in simu*.

2-2. Methods

In the present study, a simplified model in which the cell surface is represented as a 2-dimensional plane was assumed, and the cell surface was divided into subspaces. A single subspace was a cubic box with a volume of 166.1 (5.497^3) nm^3, as described previously [68]. One molecule per subspace corresponded to a concentration of 10 mM. Each calculation step was assumed to take 0.02 milliseconds. In all events of our Monte Carlo procedure, real-type pseudo uniform random numbers (N) with the range $0 \leq N < 1$ were generated, as reported previously [80]. All proteins were initially distributed into randomly selected subspaces with equal probability. When a selected subspace was occupied, the next subspace was selected randomly. Dimer formation was assumed as follows. The binding of two proteins was accepted when the two proteins occupied the neighboring subspace and N was less than $\exp(-\Delta E1/RT)$, where $\Delta E1$, R and T are the activation energy, the gas constant and the absolute temperature, respectively. Correspondingly, dimers dissociated when N was less than $\exp(-\Delta E2/RT)$.

Each protein was assumed to have a movement direction (positive or negative direction on each axis), and a diffusion rate (υ_M). In this study, the movement direction was set randomly, and υ_M were set to υ or $\upsilon/10$, where υ had a Maxwell-Boltzmann distribution from 0 to 999. The probability to have υ ($P(\upsilon)$) was calculated as follows.

$$P(\upsilon)=B(\upsilon)/S, \text{ where } S=\sum_{\upsilon=0}^{1000}B(\upsilon) \text{ and } B(\upsilon)=(2/\pi \times b^6)^{-2} \times \upsilon^2 \times \exp(-(\upsilon^2 \times b^2)/2).$$

when b was set to 0.005, a Maxwell-Boltzmann distribution of υ was obtained as shown in Fig. 2-1(a), in which P(998) and P(999) were 1 and 0, respectively. Proteins moved into their neighboring subspaces according to their directions when

$\upsilon_M > \tau$, where τ was a pseudo uniform random number ($0 \leq \tau < 1000$) obtained by multiplication of N by 1000. Its integer parts was used for the rapid simulation. When $\upsilon_M = 0$, the proteins remained in the same subspace. Proteins moved to the opposite side based on periodic boundary conditions when they reached the boundaries of simulation box. If the opposite side was occupied, the protein was reflected in the mirror direction. If the protein became a part of a dimer, the protein was allowed to pivot around its partner in a random direction. If the target subspace was occupied, the rotation was rejected and not repeated. The movement and rotation of dimers occurred at the same simulation step.

The present simulation included two events, movements and reactions for the formation and dissociation of dimers. We assumed following methods for the selection of proteins subjected to movement or reaction.

Method A = 0: Simulation processes were divided into two substeps, reaction and movement. All proteins were subjected to reaction and movement in the former and latter substeps, respectively. The reaction substep was carried out after the movement substep.

Method A = 1: Proteins were first selected to react in each step. Monomers and dimers were converted to dimers and monomers, respectively, according to the reaction probability as described above. Proteins that did not react were subjected to movement.

The moving directions of new molecules produced by the formation or the dissociation of dimers were determined randomly, and υ_M of such molecules was determined as follows.

Method B = 0: υ_M was always set to 999 .

Method B = 1: υ_M that had a Maxwell-Boltzmann distribution was set as described above.

Method B = 2: υ_M was always set to 0.

When molecules were not reacted, the moving direction and υ_M of such molecules were updated as follows.

Method C = 0: The movement directions and υ_M of all molecules were updated

in every step, and molecules moved according to their movement direction and υ_M as described above. If the subspace was occupied, the movement was rejected and not repeated.

Method C = 1: The movement direction and υ_M of 0.1 % of molecules selected randomly were updated in every step. If the subspace was occupied, the movement was rejected and not repeated.

Method C = 2: If the subspace was occupied, the molecule was reflected in the mirror direction. υ_M was not updated.

Method C = 3: If the subspace was occupied, the molecule was reflected in the mirror direction, and υ_M was updated.

Method C = 4: This method included the conditions of both Method C = 1 and Method C = 2.

Method C = 5: This model included the conditions of both Method C = 1 and Method C = 3.

The trajectories of membrane proteins are shown in Fig. 2-1(b) and (c).

Cluster size was defined as follows. All proteins presented in the neighboring subspaces are defined as belonging to the same cluster, and the cluster size was measured by counting all kinds of proteins in the cluster.

The source code of the computing program was implemented using the C-language with Visual Studio C++.net (Microsoft Co.), and the program was run on a personal computer under Windows XP or 2000 (Microsoft Co.).

2-3. Results and Discussion

In the first simulations (Fig. 2-2), the binding probabilities ($\exp(-\Delta E1/RT)$) were set as shown in Table 1. To simulate the binding rate constant (k), the simulation surface was assumed to contain 80×80 subspaces and the number of proteins was set to 960. The binding rate constant was calculated from 100 simulated values with 10 different $\Delta E1$ values. The constants were obtained with two other simulation surfaces consisting of 50×50 and 100×100 subspaces containing 750

and 500 proteins, respectively. The average values were shown in Table 1. The dissociation probabilities (exp(−ΔE2/RT)) were set to one-tenth of the binding probabilities in all simulations. The average diffusion coefficients calculated from the moving distances of 1000 proteins as described previously [68] are shown in Table 2. In this calculation, proteins are allowed to move even if the target subspace is occupied.

In the first simulation, a simulation surface consisting 80×80 subspaces and 960 monomers were set. 15 % of subspaces were occupied by proteins under these conditions. The average cluster size was the same at all binding rate constants in Method 0-1-0 (This means that Method A = 0, Method B = 1, Method C = 0) as shown in Fig. 2-2(a). This cluster may be formed without interaction between molecules at a high protein density due to proteins not being distributed uniformly at a given moment. The size of such clusters increases as the protein density increases as shown in Fig. 2-2(a), 2-3(a), and 2-4(a).

Woolf and Linderman [37] proposed that the clustering increased when the binding rate constant was high. In their simulations, molecules were first subjected to reaction and molecules that were not reacted were subjected to movement. The cluster size increased as the binding rate constant increased under their conditions (Method 1-1-0, Fig. 2-2(b)). The same results were obtained in Method 1-0-1, Method 1-1-1, Method 1-1-5 (data not shown). In this method (Method A = 1), monomers dissociated from dimers do not move because these monomers are not selected for movement. In the next step, a large proportion of such monomers are selected again to form dimers when the binding rate constant is high. This means that a large proportion of dissociated monomers form dimers again without moving at the next step. Therefore, the cluster size is larger at a high binding rate constant. In contrast, when the reaction and movement events are repeated at every step (Method A = 0), dissociated monomers have the same potential to associate as monomers formed in previous steps. The same results were obtained with different protein densities except that the cluster size and number of dimers increased as the density increased (Fig. 2-4(a) and (b)). To confirm this explanation, moving energy

of dissociated monomers was set to zero in Method A = 0, i.e., such monomers do not move in the next step. As shown in Fig. 2-2(c), the cluster size increased as the binding rate constant increased.

The increase in the cluster size accompanies a decrease in entropy. In the simple model used in this simulation, no additional energy was supplied for the decrease in entropy when the binding rate constant increased. Therefore, it is reasonable to assume that cluster size is constant at any binding rate constant, suggesting that Method A = 1 is inadequate. Method B = 0 and Method B = 2 seem to be far removed from natural conditions. Therefore, Method A = 0 and Method B = 1 seem to be adequate.

The next point is which method is appropriate in Method C. In the method described above, the diffusion rates and movement directions of all molecules were updated immediately before the movement in every step. However, it is more reasonable to assume that each molecule has a different molecule activity, namely a different diffusion rate, and keeps the same energy for a while. Therefore, namely Method C = 0 is less likely.

The question is thus when molecular activity changes. We first assume that 0.1 % of molecules selected randomly were updated in every step (Method C = 1). The average cluster size decreased as the binding rate constant increased in these conditions, while the decrease in the number of dimers was small (Fig. 2-2(d)). This decrease was similar when the density of proteins increased 2-fold (Fig. 2-3(c)) and small at a low density of proteins (Fig. 2-4(c)). In this simulation, when a protein ran against another protein, its movement was cancelled and its movement direction was not updated. When the binding rate constant was high, each such protein formed a dimer with its neighboring protein immediately, and the movement direction of the dimer was newly assigned. Consequently, the dimer moved away, resulting in a decrease in the cluster size. In contrast, when the binding rate constant was low, proteins that ran against another protein in cluster stayed in the same subspaces for a long time until the proteins were subjected to reaction. This may be the reason for the increase in cluster size at a low binding

rate constant.

It is likely that the molecular energy is changed when a collision between molecules occurs in the natural case. In the next simulation, the diffusion direction was updated only when a protein ran against another protein (Method C = 2). The average cluster size was the same for all binding rate constants (Fig. 2-2(e)). The same results were obtained when both diffusion rate and direction were updated only when a molecule ran into another molecule (Method C = 3, Fig. 2-2(f)). It is likely that energy is released in a open space even if there is no collision. The same results were obtained in Method C = 4 and 5 which included the updating of 0.1 % of molecules at every step (Method C = 1) in addition to the conditions of Method C = 2 and 3, respectively (Fig. 2-2(g) and (h)). The cluster sizes were the same again in Method C = 2 to 5 at the protein densities described in Fig. 2-3 and 2-4 (data obtained with Method C = 2 to 4 are not shown).

The binding rate constants measured experimentally were less than 1×10^7 M^{-1} sec^{-1} [81-84]. When the binding rate constant was less than 5×10^6 M^{-1} sec^{-1}, all methods used in the present simulation gave the similar results except Method 0-1-1 (Fig. 2-2, 2-3, 2-4). However, it may be better to use Method 0-1-5.

In Method C = 1, 4 and 5, 0.1 % of proteins selected randomly were updated in every step. It remains unclear whether this setting is the most appropriate or not. The trajectories in Method C = 5 (Fig. 2-1(c)) were similar to those observed experimentally [85]. Although more detailed experimental data are required for more proper setting, 0.1 % is probably appropriate.

When the diffusion coefficient of molecules was increased 10 fold ($\upsilon_M = \upsilon$), similar results were obtained except that the cluster size decreased more dramatically as the binding rate constant increased as compared with the lower diffusion coefficient (Fig. 2-5(c)). The diffusion coefficient of membrane proteins observed experimentally was 0.1 to 0.3 μm^2 sec^{-1} in prokaryotes [86] and eukaryotes [87, 88], and the diffusion coefficient in the setting of $\upsilon_M = \upsilon$ was 12.8 μm^2 sec^{-1} in Method C = 1. Therefore, this setting may be less appropriate. It should be noted that the same diffusion coefficient was obtained in Method C = 1

to 5 because proteins were allowed to move even if the target subspace was occupied when the diffusion coefficient was calculated.

Our present simulation with appropriate algorithms demonstrated that the cluster size was dependent on neither the diffusion coefficient nor the binding speed of proteins at all protein densities tested. Thus, the self-assembly induced by protein dimerization with a high binding speed is unlikely *in situ*.

GPCRs have been shown to form not only dimers but also oligomers [74, 89-91], but structural studies of these receptors have suggested them to have only one protein-protein binding site [92]. It may be possible for a membrane protein complex to be formed without such binding site. One possibility is that the hydrophilic surface regions of membrane proteins might bind each other in the membranes. Another possibility is that matrix proteins in outer or inner cell surface trap membrane proteins in a local area to increase the protein density. It was observed that membrane proteins undergoing Brownian diffusion were confined within a limited area, probably by the binding to a membrane -associated cytoskeleton network [93]. In any case, some interactions between proteins may be required for the cluster formation of membrane proteins on the cell surface at a low protein density observed experimentally.

We examined the cluster formation with Monte Carlo simulation using two algorithms. The first one was that simulation processes were divided into two substeps. All proteins were subjected to movement in the first substep, and then subjected to reaction in the second substep. The second algorithm was that proteins were first selected to react and then proteins that did not react were subjected to movement in each step. The self-assembly induced by protein dimerization with a high binding speed, which was claimed by Woolf and Linderman [37], was simulated with the second algorithm, while the cluster size was dependent on neither the diffusion coefficient nor the binding speed of proteins with the first algorithm. In the second algorithm, monomers dissociated from dimmers do not move because these monomers are not selected for movement, and a large proportion of such monomers are selected to form dimers before their movements

in the next step. The self-organization was again stimulated in the former algorithm containing the conditions that the monomers dissociated from dimers did not move in the next movement substep. This algorithm seems to be far removed from natural conditions. Thus, it is inferred that the self-assembly induced by protein dimerization is unlikely *in simu*, and that some interaction between proteins is required for the cluster formation.

The second algorithm has been used in many previous works, but the present simulation suggests that the first one is more appropriate. We also examined which algorithm was more appropriate for the molecular movement. It has been assumed in many previous simulations that molecules move to the neighboring subspace randomly in each simulation step. In this study, it was shown to be more appropriate that molecules continued to have the same direction for a while and the direction was changed at the step selected randomly. Many previous studies adopted the algorithm that movement was cancelled when the collision occurred. The present study demonstrated that this algorithm was less appropriate, and molecules should change their movement direction in a mirror manner when the neighboring subspace was occupied. It should be clarified in future simulations which interaction is required for clustering of membrane proteins observed experimentally using these appropriate methods.

Table 1. Binding rate constants

Δ E1/RT*	binding probability	binding rate constants (k)**	log (k)
0.01	0.99	$(1.04\pm0.32)\times10^{7}$	7.02
0.11	9.0×10^{-1}	$(9.75\pm2.90)\times10^{6}$	6.99
1.20	3.0×10^{-1}	$(4.51\pm0.68)\times10^{6}$	6.65
2.41	9.0×10^{-2}	$(1.61\pm0.07)\times10^{6}$	6.21
3.50	3.0×10^{-2}	$(5.45\pm0.42)\times10^{5}$	5.74
4.71	9.0×10^{-3}	$(1.58\pm0.06)\times10^{5}$	5.20
5.81	3.0×10^{-3}	$(5.38\pm0.51)\times10^{4}$	4.73
7.01	9.0×10^{-4}	$(1.60\pm0.07)\times10^{4}$	4.20
8.11	3.0×10^{-4}	$(5.66\pm0.31)\times10^{3}$	3.75
9.32	9.0×10^{-4}	$(1.64\pm0.05)\times10^{3}$	3.21

*see Methods
**$M^{-1}\bullet sec^{-1}$

Table 2. Diffusion coefficients

Method C	υ_M	Diffusion coefficients ($\mu m^2/s$)
0	υ	0.166 ± 0.005
0	$\upsilon/10$	0.0169 ± 0.0004
1	υ	12.8 ± 0.5
1	$\upsilon/10$	0.145 ± 0.003

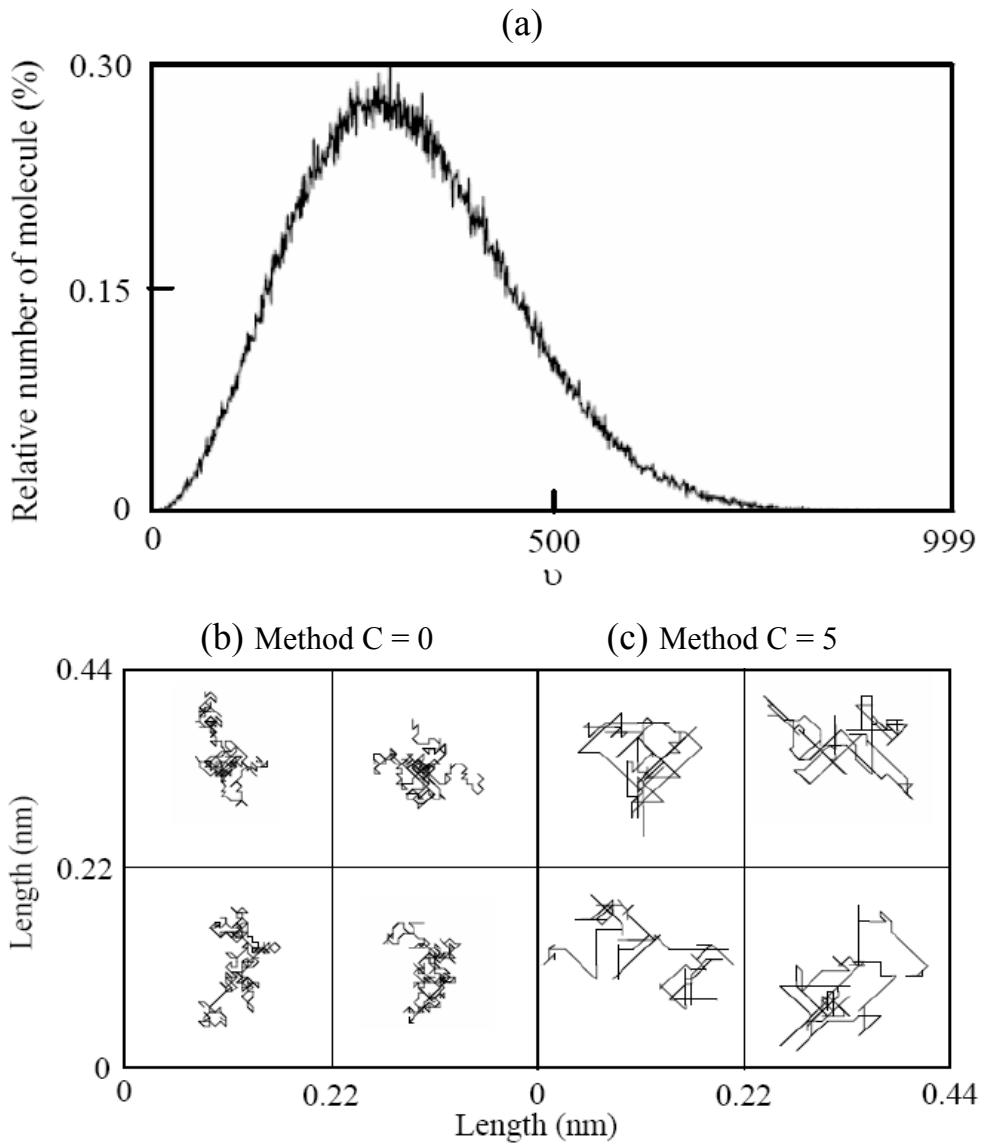

Figure 2-1. Distribution of diffusion rates and trajectories of membrane protein movement.

(a) Distribution of diffusion rates. (b) and (c) The position of a given protein were plotted for 1×10^5 steps (2 sec) at interval of 10 steps (0.2 msec). Method C = 0 (b) and Method C = 5 (c) were used. The numbers of subspaces and proteins set in this simulation were 80×80 and 960, respectively.

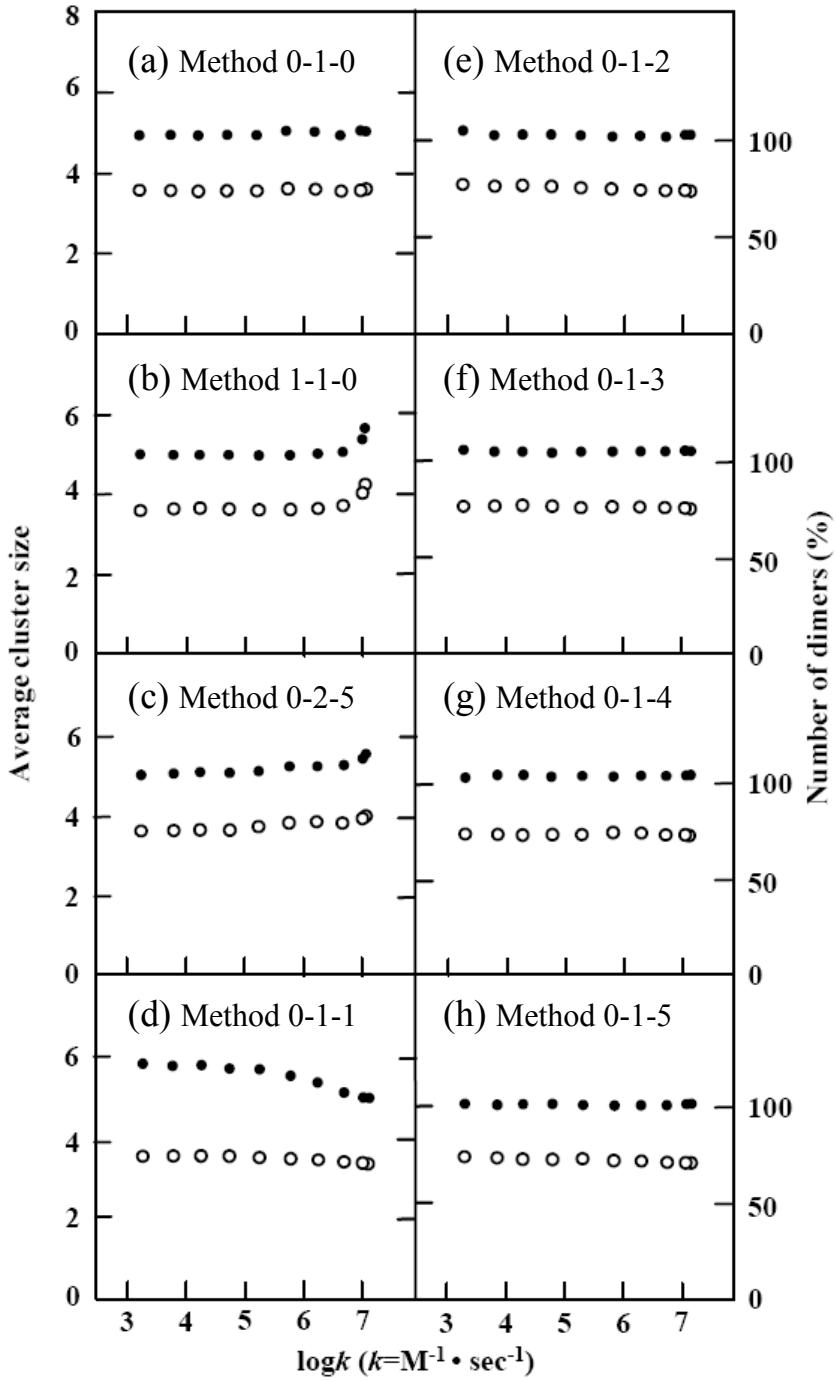

Figure 2-2. The average clustering size and the number of dimers when the molecular density was 4950 proteins per mm^2 and υ_M was υ/10.

The cell surface consisted of 80×80 subspaces, and the number of proteins was initially set to 960. 15 % of subspaces were initially occupied with proteins. The diffusion rates of proteins (υ_M) were set υ/10. Methods used are indicated in the figures. After the reaction reached equilibrium stage, the total number of monomers and dimers was calculated in each cluster at each step, and average value was obtained (closed circles). The number of dimers at each step was calculated and average percentage of proteins that formed dimers was obtained (open circles). Each point represents the average values obtained from 100 measurements, and standard deviations were less than 5 % in all measurements. The horizontal line represents the binding rate constant (k).

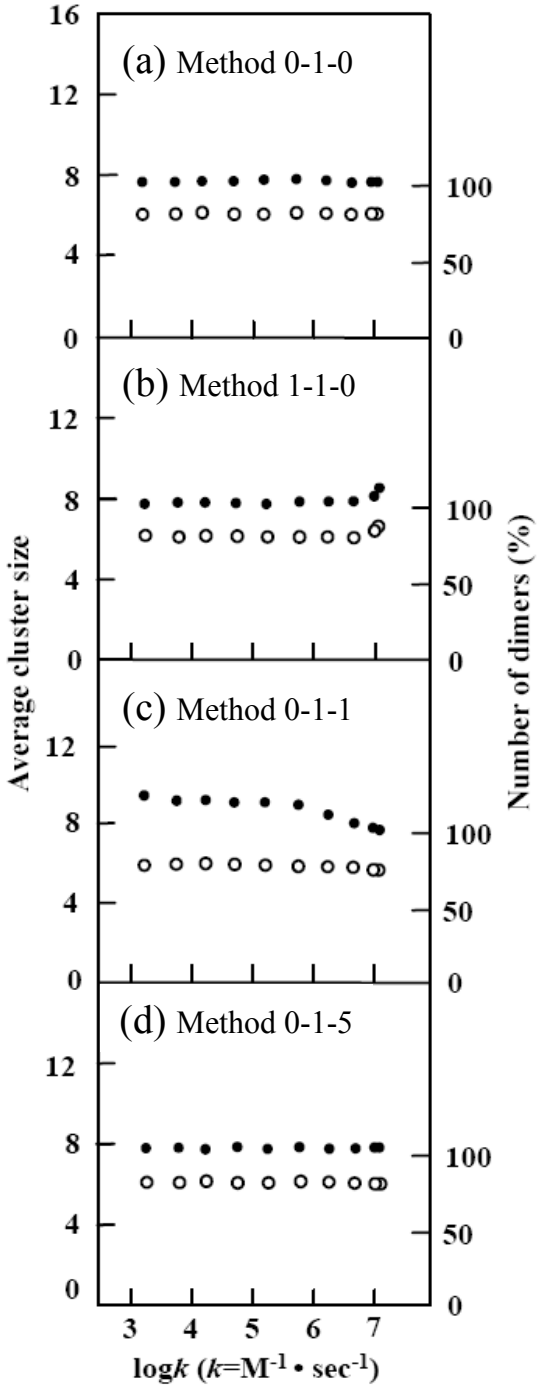

Figure 2-3. The average cluster size and the number of dimers when the molecular density was 9900 proteins per μm^2 and υ_M was $\upsilon/10$.

The simulation conditions were the same as in Figure 2-2 except that the cell surface consisted of 50×50 subspaces and the number of proteins was initially set to 750. 30 % of subspaces were initially occupied by proteins.

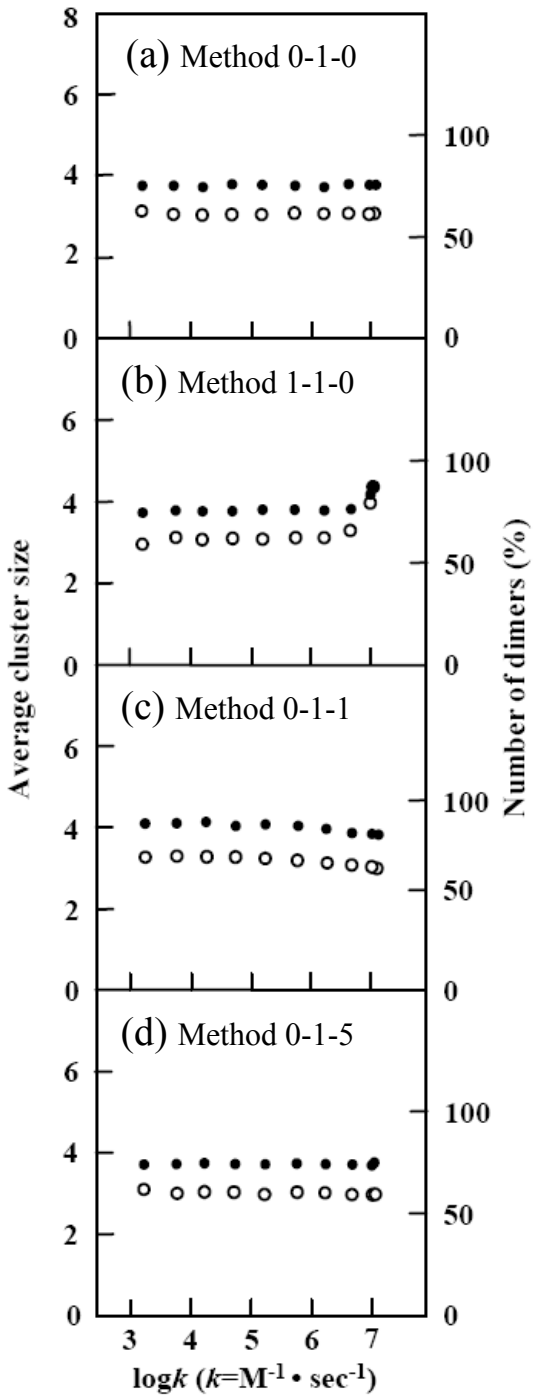

Figure 2-4. The average cluster size and the number of dimers when the molecular density was 1650 proteins per μm^2 and υ_M was υ/10.

The simulation conditions were the same as in Figure 2-2 except that the cell surface consisted of 100×100 subspaces and the number of proteins was initially set to 500. 5 % of subspaces were initially occupied by proteins.

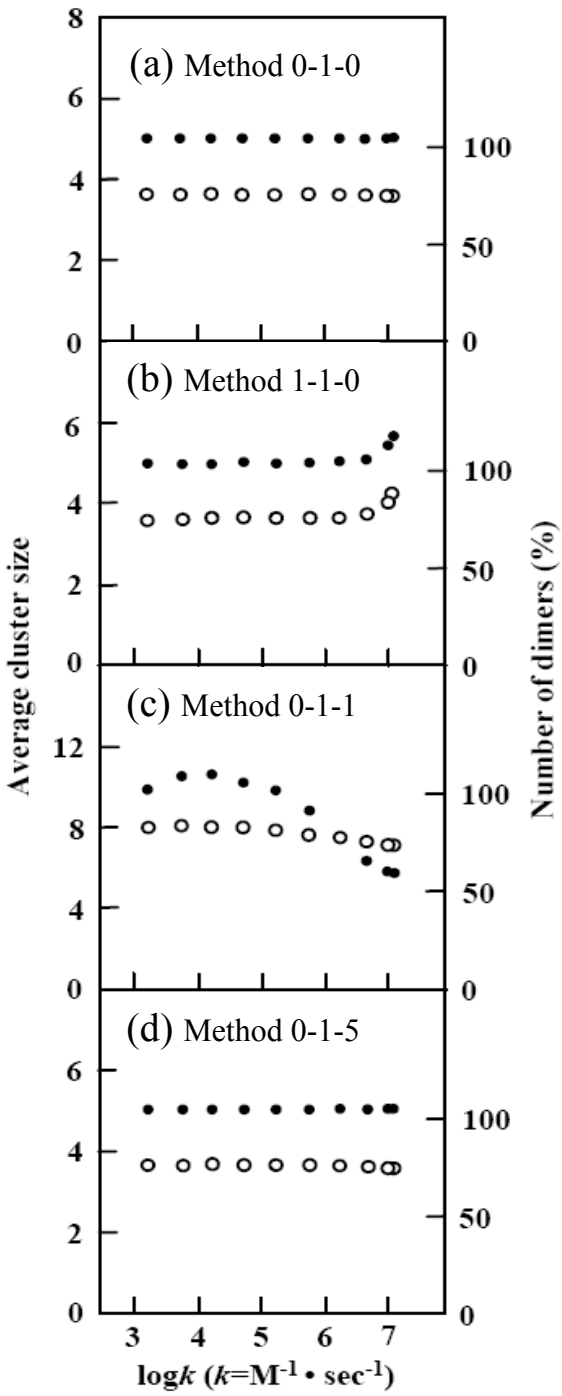

Figure 2-5. The average cluster size and the number of dimers when the molecular density was 4950 proteins per μm^2 and υ_M was υ/10.

The simulation conditions were the same as in Figure 2-2 except that the diffusion rate of proteins (υ_M) was set to υ.

CONCLUSIONS

In this study, the effect of extracellular acidic pH on TCR signaling was examined with Jurkat T cells and human T cells from peripheral blood. It had found that in Jurkat T cells that (1) after CD3 stimulation TCR signaling followed by ZAP-70, ERK and p38 was more active, (2) Ca^{2+} mobilization was more strongly induced by CD3 stimulation through ZAP-70 and LAT, but not SLP-76, while CD28 costimulation attenuated the Ca^{2+} mobilization at acidic pH, and (3) IL-2 expression was not induced by the activation of TCR signaling under acidic conditions. In human T cells from peripheral blood, the initial step of TCR signaling and Ca^{2+} mobilization induced by CD3 were weaker in acidic environments. These data showed that TCR signaling pathways initiated by CD3 stimulation are different in parts under different pH conditions.

It was found in this study that the clustering by the self-assembly was not simulated when an appropriate algorithm was used, suggesting that some protein-protein interaction is essential for the clustering of the TCR complex. In addition, it was suggested experimentally that different clusters may be formed under different pH conditions.

REFERENCES

[1] **Dubos, R.J.** (1955) The micro-environment of inflammation or Metchnikoff revisited. *Lancet* 269: 1-5.

[2] **Lardner, A.** (2001) The effects of extracellular pH on immune function. *J Leukoc Biol* 69: 522-530.

[3] **Martin, G.R., Jain, R.K.** (1994) Noninvasive measurement of interstitial pH profiles in normal and neoplastic tissue using fluorescence ratio imaging microscopy. *Cancer Res* 54: 5670-5674.

[4] **Simmen, H.P., Blaser, J.** (1993) Analysis of pH and pO2 in abscesses, peritoneal fluid, and drainage fluid in the presence or absence of bacterial infection during and after abdominal surgery. *Am J Surg* 166: 24-27.

[5] **Grimshaw, M.J., Balkwill, F.R.** (2001) Inhibition of monocyte and macrophage chemotaxis by hypoxia and inflammation--a potential mechanism. *Eur J Immunol* 31: 480-489.

[6] **Gerweck, L.E., Seetharaman, K.** (1996) Cellular pH gradient in tumor versus normal tissue: potential exploitation for the treatment of cancer. *Cancer Res* 56: 1194-1198.

[7] **Helmlinger, G., Yuan, F., Dellian, M., Jain, R.K.** (1997) Interstitial pH and pO_2 gradients in solid tumors in vivo: high-resolution measurements reveal a lack of correlation. *Nat Med* 3: 177-182.

[8] **Stubbs, M., McSheehy, P.M., Griffiths, J.R., Bashford, C.L.** (2000) Causes and consequences of tumor acidity and implications for treatment. *Mol Med Today* 6: 15-19.

[9] **Kudoh, S., Redovan, C., Rayman, P., Edinger, M., Tubbs, R.R., et al.** (1997) Defective granzyme B gene expression and lytic response in T lymphocytes infiltrating human renal cell carcinoma. *J Immunother* 20: 479-487.

[10] **Liao, Y.P., Schaue, D., McBride, W.H.** (2007) Modification of the tumor microenvironment to enhance immunity. *Front Biosci* 12: 3576-3600.

[11] **Winkler, A.E., Brotman, J.J., Pittman, M.E., Judd, N.P., Lewis, J.S. Jr., et al.** (2011) CXCR3 enhances a T cell dependent epidermal proliferative response and promotes skin tumorgenesis. *Cancer Res* 71: 5707-5716.

[12] **Chechneva, O.V., Mayrhofer, F., Daugherty, D.J., Pleasure, D.E., Hong, J.S., et al.** (2011) Low dose dextromethorphan attenuates moderate experimental autoimmune encephalomyelitis by inhibiting NOX2 and reducing peripheral immune cells infiltration in the spinal cord. *Neurobiol Dis* 44: 63-72.

[13] **Koelle, D.M., Benedetti, J., Langenberg, A., Corey, L.** (1992) Asymptomatic reactivation of herpes simplex virus in women after the first episode of genital herpes. *Ann Intern Med* 116: 433-437.

[14] **Bidani, A., Wang, C.Z., Saggi, S.J., Heming, T.A.** (1998) Evidence for pH sensitivity of tumor necrosis factor-alpha release by alveolar macrophages. *Lung* 176: 111-121.

[15] **Grabowski, J.E., Vega, V.L., Talamini, M.A., De Maio, A.** (2008) Acidification enhances peritoneal macrophage phagocytic activity. *J Surg Res* 147: 206-211.

[16] **Trevani, A.S., Andonegui, G., Giordano, M., López, D.H., Gamberale, R., et al.** (1999) Extracellular acidification induces human neutrophil activation. *J Immunol* 162: 4849-4857.

[17] **Müller, B., Fischer, B., Kreutz, W.** (2000) An acidic microenvironment impairs the generation of non-major histocompatibility complex-restricted killer cells. *Immunology* 99: 375-384.

[18] **Vermeulen, M., Giordano, M., Trevani, A.S., Sedlik, C., Gamberale, R., et al.** (2004) Acidosis improves uptake of antigens and MHC class I-restricted presentation by dendritic cells. *J Immunol* 172: 3196-3204.

[19] **Martínez, D., Vermeulen, M., von Euw, E., Sabatté, J., Maggíni, J., et al.** (2007) Extracellular acidosis triggers the maturation of human dendritic cells and the production of IL-12. *J Immunol* 179: 1950-1959.

[20] **Fukamachi, T., Saito, H., Kakegawa, T., Kobayashi, H.** (2002) Different proteins are phosphorylated under acidic environments in Jurkat cells. *Immunol Lett* 82: 155-158.

[21] **Hirata S, Fukamachi T, Sakano H, Tarora A, Saito H, et al.** (2008) Extracellular acidic environments induce phosphorylation of ZAP-70 in Jurkat T cells. *Immunol Letters* 115: 105-109.

[22] **Horejsi, V.** (2003) The roles of membrane microdomains (rafts) in T cell activation. *Immunol Rev* 191: 148-164.

[23] **Luna, E.J., Hitt, A.L.** (1992) Cytoskeleton-plasma membrane interactions. *Science* 258: 955-964.

[24] **Zacharias, D.A., Violin, J.D., Newton, A.C., Tsien, Y.R.** (2002) Partitioning of lipid-modified monomeric GFPs into membrane microdomains of live cells. *Science* 296: 913-916.

[25] **Sharma, P., Varma, R., Sarasij, R.C., Ira Gousset, K., Krishnamoorthy, G.G., et al.** (2004) Nanoscale organization of multiple GPI-anchored proteins in living cell membranes. *Cell* 116: 577-589.

[26] **Leksa, V., Godar, S., Schiller, H.B., Fuertbauer, E., Muhammad, A., et al.** (2005) TGF-beta-induced apoptosis in endothelial cells mediated by M6P/IGFII-R and mini-plasminogen. *J Cell Sci* 118: 4577-4586

[27] **Simons, K., Ikonen, E.** (1997) Functional rafts in cell membranes. *Nature* 387: 569-572.

[28] **Rietveld, A., Simons, K.** (1998) The differential miscibility of lipids as the basis for the formation of functional membrane rafts. *Biochim Biophys Acta* 1376: 467-479.

[29] **Lillemeier, B.F., Pfeiffer, J.R., Surviladze, Z., Wilson, B.S., Davis, M.M.** (2006) Plasma membrane-associated proteins are clustered into islands attached to the cytoskeleton. *Proc Natl Acad Sci USA* 103: 18992-18997.

[30] **Smith-Garvin, J.E., Koretzky, G.A., Jordan, M.S.** (2009) T cell activation. *Annu Rev Immunol* 27: 591-619.

[31] **Molnar, E., Dopfer, E.P., Deswal, S., Schamel, W.W.** (2009) Models of antigen receptor activation in the design of vaccines. *Curr Pharm Des* 15: 3237-3248.

[32] **Molnar, E., Deswal, S., Schamel, W.W.** (2010) Pre-clustered TCR complexes. *FEBS Lett* 583: 4832-4837.

[33] **Schamel, W.W., Arechaga, I., Risueno, R.M., van Santen, H.M., Cabezas, P., et al.** (2005) Coexistence of multivalent and monovalent TCRs explains high sensitivity and wide range of response. *J Exp Med* 202: 493-503.

[34] **Wilson, B.S., Pfeiffer, J.R., Surviladze, Z., Gaudet, E.A., Oliver, J.M.** (2001) High resolution mapping of mast cell membranes reveals primary and secondary domains of Fc(epsilon)RI and LAT. *J Cell Biol* 154: 645-658.

[35] **Lillemeier, B.F., Mortelmaier, M.A., Forstner, M.B., Huppa, J.B., Groves, J.T., et al.** (2010) TCR and Lat are expressed on separate protein islands on T cell membranes and concatenate during activation. *Nat Immunol* 11: 90-96.

[36] **Sanchez-Lockhart, M., Miller, J.** (2006) Engagement of CD28 outside of immunological synapses results in up-regulation of IL-2 mRNA stability but not IL-2 transcription. *J Immunol* 176: 4778-4784.

[37] **Woolf, P.J., Linderman, J.J.** (2003) Self organization of membrane proteins via dimerization. *Biophys Chem* 104: 217-227.

[38] **Latour, S., Veillette, A.** (2001) Proximal protein tyrosine kinases in immuno--receptor signaling. *Curr Opin Immunol* 13: 299-306.

[39] **Chae, H-D., Siefring, J.E., Hildeman, D.A., Gu, Y., Williams, D.A.** (2010) RhoH Regulates Subcellular Localization of ZAP-70 and Lck in T Cell Receptor Signaling. *PLoS ONE* 5: e13970.

[40] **Krishnan, S., Warke, V.G., Nambiar, M.P., Tsokos, G.C., Farber, D.L.** (2003) The FcRγ Subunit and Syk Kinase Replace the CD3ζ-Chain and ZAP-70 Kinase in the TCR Signaling Complex of Human Effector CD4 T Cells. *Immunol* 170: 4189-4195.

[41] **van Leeuwen, J.E., Samelson, L.E.** (1999) T cell antigen-receptor signal transduction. *Curr Opin Immunol* 11: 242-248.

[42] **Feske, S.** (2007) Calcium signalling in lymphocyte activation and disease. *Nat Rev Immunol* 7: 690-702.

[43] **Feske, S., Giltnane, J., Dolmetsch, R., Staudt, L.M., Rao, A.** (2001) Gene regulation mediated by calcium signals in T lymphocytes. *Nat Immunol* 2: 316-324.

[44] **Dolmetsch, R.E., Lewis, R.S., Goodnow, C.C., Healy, J.I.** (1997) Differential activation of transcription factors induced by Ca^{2+} response amplitude and duration. *Nature* 386: 855-858.

[45] **Boothby, M.** (2010) CRACking the code without Rosetta: molecular regulation of calcium-stimulated gene transcription after T cell activation. *J Immunol* 185: 4969-4971.

[46] **Grynkiewicz, G., Poenie, M., Tsien, R.Y.** (1985) A new generation of Ca^{2+} indicators with greatly improved fluorescence properties. *J Biol Chem* 260: 3440-3450.

[47] **Freedman, B.D., Liu, Q.H., Somersan, S., Kotlikoff, M.I., Punt, J.A.** (1999) Receptor avidity and costimulation specify the intracellular Ca^{2+} signaling pattern in $CD4^{+}CD8^{+}$ thymocytes. *J Exp Med* 190: 943-952.

[48] **Michel, F., Attal-Bonnefoy, G., Mangino, G., Mise-Omata, S., Acuto, O.** (2001) CD28 as a molecular amplifier extending TCR ligation and signaling capabilities. *Immunity* 15: 935-945.

[49] **Zitt, C., Strauss, B., Schwarz, E.C., Spaeth, N., Rast, G., et al.** (2004) Potent inhibition of Ca^{2+} release-activated Ca^{2+} channels and T-lymphocyte activation by the pyrazole derivative BTP2. *J Biol Chem* 279: 12427-12437.

[50] **Williams, B.L., Schreiber, K.L., Zhang, W., Wange, R.L., Samelson, L.E., et al.** (1998) Genetic evidence for differential coupling of Syk family kinases to the T-cell receptor: reconstitution studies in a ZAP-70-deficient Jurkat T-cell line. *Mol Cell Biol* 18: 1388-1399.

[51] **Yablonski, D., Kuhne, M.R., Kadlecek, T., Weiss, A.** (1998) Uncoupling of nonreceptor tyrosine kinases from PLC-gamma1 in an SLP-76-deficient T cell. *Science* 281: 413-416.

[52] **Brdicka, T., Imrich, M., Angelisová, P., Brdicková, N., Horváth, O., et al.** (2002) Non-T cell activation linker (NTAL): a transmembrane adaptor protein involved in immunoreceptor signaling. *J Exp Med* 196: 1617-1626.

[53] **June, C.H., Rabinovitch, P.S. and Ledbetter, J.A.** (1987) CD5 antibodies increase intracellular ionized calcium concentration in T cells. *J Immunol* 138: 2782-2792.

[54] **Zhang, J., Salojin, K.V., Gao, J.X., Cameron, M.J., Bergerot, I., et al.** (1999) p38 mitogen-activated protein kinase mediates signal integration of TCR/CD28 costimulation in primary murine T cells. *J Immunol* 162: 3819-3829.

[55] **Shan, X., Balakir, R., Criado, G., Wood, J.S., Seminario, M.C., et al.** (2001) Zap-70-independent Ca^{2+} mobilization and Erk activation in Jurkat T cells in response to T-cell antigen receptor ligation. *Mol Cell Biol* 21: 7137-7149.

[56] **Hogan, P.G., Chen, L., Nardone, J., Rao, A.** (2003) Transcriptional regulation by calcium, calcineurin, and NFAT. *Genes Dev* 17: 2205-2232.

[57] **Frantz, B., E. C. Nordby, G. Bren, N. Steffan, C. V. Paya, et al.** (1994) Calcineurin acts in synergy with PMA to inactivate I kappa B/MAD3, an inhibitor of NF-kappa B. *EMBO J* 13:861-870.

[58] **Jain, J., Loh, C., Rao, A.** (1995) Transcriptional regulation of the IL-2 gene. *Curr Opin Immunol* 7: 333-342.

[59] **Umlauf, S.W., Beverly, B., Lantz, O., Schwartz, R.H.** (1995) Regulation of interleukin 2 gene expression by CD28 costimulation in mouse T-cell clones: both nuclear and cytoplasmic RNAs are regulated with complex kinetics. *Mol Cell Biol* 15: 3197-3205.

[60] **Darnel, J., Lodish, H., Baltimore, D.** (1986) Molecular Cell Biology, Scientific American Books Inc., New York.

[61] **Harding, F., McArthur, J., Gross, J., Raulet, D., Allison, J.** (1992) CD28--mediated signalling co-stimulates murine T cells and prevents induction of anergy in T-cell clones. *Nature* 356: 607-609.

[62] **Sanchez-Lockhart, M., Miller, J.** (2006) Engagement of CD28 outside of the immunological synapse results in up-regulation of IL-2 mRNA stability but not IL-2 transcription. *J Immunol* 176: 4778-4784.

[63] **Bustelo, X.R.** (2001) Vav proteins, adaptors and cell signaling. Oncogene 20: 6372-6381

[64] **Fraser, J., Irving, B., Crabtree, G., Weiss, A.** (1991) Regulation of interleukin-2 gene enhancer activity by the T cell accessory molecule CD28. *Science* 251: 313-316.

[65] **Lindsten, T., June, C.H., Ledbetter, J.A., Stella, G., Thompson, C.B.** (1989) Regulation of lymphokine messenger RNA stability by a surface-mediated T cell activation pathway. *Science* 244: 339-343.

[66] **Rulifson, I., Sperling, A., Fields, P., Fitch, F., Bluestone, J.** (1997) CD28 costimulation promotes the production of Th2 cytokines. *J Immunol* 158: 658-665.

[67] **Fukamachi, T., Chiba, Y., Wang, X., Saito, H., Tagawa, M., et al.** (2010) Tumor specific low pH environments enhance the cytotoxicity of lovastatin and cantharidin. *Cancer Lett* 297: 182-189.

[68] **Kobayashi, H., Azuma, R., Yasunaga, T.** (2009) Expression of excess receptors and negative feedback control of signal pathways are required for rapid activation and prompt cessation of signal transduction. *Cell Commun Signal* 7:3.

[69] **Brinkerhoff, C.J., Woold, P.J., Linderman, J.J.** (2004) Monte Carlo simulations of receptor dynamics: insights into cell signaling. *J Mol Hiosol* 35:

667-677.

[70] **Kobayashi, H., Azuma, R., Konagaya, A.** (2007) Clustering of membrane proteins in the pre-stimulation stage is required for signal transduction: a computer analysis. *Signal transduction* 7: 329-339.

[71] **Costa, M.N., Radhakrishnan, K., Edwards, J.S.** (2011) Monte Carlo simulations of plasma membrane corral-induced EGFR clustering. *J Biotech* 151: 261-270.

[72] **Srinivas, R.A., Tsourkas, P.K., Raychaudhuri, S.** (2011) Monte Carlo study of B-cell receptor clustering mediated by antigen crosslinking and directed transport. *Cell Mol Immunol* 8: 255-264.

[73] **Yu, X., Sharma, K.D., Takahashi, T., Iwamoto, R., Mekada, E.** (2002) Ligand-independent dimer formation of epidermal growth factor receptor (EGFR) is a step separable from ligand-induced EGFR signaling. *Mol Biol Cell* 13: 2547-2557.

[74] **Hebert, T.E., Bouvier, M.** (1998) Structural and functional aspects of G protein-coupled receptor oligomerization. *Biochem Cell Biol* 76: 1-11.

[75] **Gomes, I., Jordan, B.A., Gupta, A., Rios, C., Trapaidze, N., et al.** (2001) G protein coupled receptor dimerization: implications in modulating receptor function. *J Mol Med* 79: 226-242.

[76] **Kusumi, A., Koyama-Honda, L., Suzuki. K.** (2004) Molecular dynamics and interactions for creation of stimulation-induced stabilized rafts from small unstable rafts. *Traffic* 5: 213-230.

[77] **Gimborn, K., Lessmann, E., Kuppig, S., Krystal, G., Huber, M.** (2005) SHIP down-regulates FcepsilonR1-induced degranulation at supraoptimal IgE or antigen levels. *J Immunol* 174: 507-516.

[78] **Lesourne, R., Fridman, W.H., Daeron, M.** (2005) Dynamic interactions of Fc gamma receptor IIB with filaminbound SHIP1 amplify filamentous actin-dependent negative regulation of Fc epsilon receptor I signaling. *J Immunol* 174: 1365-1373.

[79] **Meakin, P.** (1986) Multiple-contact diffusion-limited-aggregation model. *Phys Rev A* 33: 4199-4204.

[80] **Matsumoto, M., Nishimura, T.** (1998) Mersenne twister: A 623-dimensionally equidistributed uniform pseudo-random number generator. *ACM Transactions on*

Modeling and Computer Simulation 8: 3-30.

[81] **Andrews, A.L., Holloway, J.W., Puddicombe, S.M., Holgate, S.T., Davies, D.E.** (2002) Kinetic analysis of the interleukin-13 receptor complex. *J Biol Chem* 277: 46073-46078.

[82] **Felder, S., LaVin, J., Ullrich, A., Schlessinger, J.** (1992) Kinetics of binding, endocytosis, and recycling of EGF receptor mutants. *J Cell Biol* 117: 203-212.

[83] **Wilkinson, J.C., Stein, R.A., Guyer, C.A., Beechem, J.M., Staros, J.V.** (2001) Real-time kinetics of ligand/cell surface receptor interactions in living cells: binding of epidermal growth factor to the epidermal growth factor receptor. *Biochemistry* 40: 10230-10242.

[84] **Teramura, Y., Ichinose, J., Takagi, H., Nishida, K., Yanagida, T., Sako, Y.** (2001) Single-molecule analysis of epidermal growth factor binding on the surface of living cells. *EMBO J* 25: 4215-4222.

[85] **Kusumi, A., Shirai, Y.M., Koyama-Honda, I., Suzuki, K.G.N., Fujiwara, T.K.** (2010) Hierarchical organization of the plasma membrane: Investigations by single-molecule tracking vs. fluorescence correlation spectroscopy. *FEBS lett* 584: 1814-1823.

[86] **Mullineaux, C.W., Nenninger, A., Ray, N., Robinson, C.** (2006) Diffusion of green fluorescent protein in three cell environments in *Escherichia coli*. *J Bacteriol* 188: 3442-3448.

[87] **Ishihara, A., Hou, Y., Jacobson, K.** (1987) The Thy-1 antigen exhibits rapid lateral diffusion in the plasma membrane of rodent lymphoid cells and fibroblasts. *Proc Natl Acad Sci USA* 84: 1290-1293.

[88] **Zhang, F., Crise, B., Su, B., Hou, Y., Rose, J.K., Bothwell, A., Jacobson, K.** (1991) Lateral diffusion of membrane-spanning and glycosyl phosphatidyl--inositol-linked proteins: toward establishing rules governing the lateral mobility of membrane proteins. *J Cell Biol* 115: 75-84.

[89] **George, S.R., Fan, T., Xie, Z., Tse, R., Tam, V., Varghese, G., O'Dowd, B.F.** (2000) Oligomerization of mu- and delta-opioid receptors.Generation of novel functional properties. *J Biol Chem* 275: 26128-26135.

[90] **Nimchinsky, E.A., Hof, P.R., Janssen, W.G.M., Morrison, J.H., Schmauss, C.** (1997) Expression of dopamine D3 receptor dimers and tetramers in brain and in transfected cells. *J Biol Chem* 272: 29229-29237.

[91] **Park, P., Sum, C.S., Hampson, D.R., Van Tol, H.H., Wells, J.W.** (2001) Nature of the oligomers formed by muscarinic m2 acetylcholine receptors in Sf9 cells. *Eur J Pharmacol* 421: 11-22.

[92] **Maggio, R., Barbier, P., Colelli, A., Salvadori, F., Demontis, G., et al.** (1999) G protein-linked receptors: pharmacological evidence for the formation of heterodimers. *J Pharmacol Exp Ther* 291: 251-257.

[93] **Kusumi, A., Sako, Y., Yamamoto, M.** (1993) Confined lateral diffusion of membrane receptors as studied by single partical tracking (nanovid microscopy). Effects of calcium-induced differentiation in cultured epithelial cells. *Biophysical Journal* 65: 2021-2040.

LIST OF PUBLICATIONS

This doctoral thesis was written by re-constructing with the following manuscripts.

1. Xin Wang，Toshihiko Fukamachi, Hiromi Saito, Hiroshi Kobayashi. Do membrane proteins cluster without binding between molecules? Open Journal of Immunology. 2:1-8 (2012).

2. Xin Wang, Kenta Hatatani, Yirong Sun, Toshihiko Fukamachi, Hiromi Saito, Hiroshi Kobayashi. TCR signaling via ZAP-70 induced by CD3 stimulation is more active under acidic conditions. Journal of Cell Science & Therapy. (In press).

ACKNOWLEDGEMENTS

First and foremost, I would like to express my deepest gratitude to Professor Hiroshi Kobayashi, My supervisor, for his constant encouragement and guidance. He has walked me through all the stages of writing this thesis. Without his consistent and illuminating instructions, this thesis could not reach its present form.

Next my sincere thanks goes to Professor Masatoshi Tagawa and Professor Motoyuki Ito for the constructive advice, guidance and encouragement during the last one year of this research. I would like to express my grateful gratitude to Dr. Hiromi Saito and Dr. Toshihiko Fukamachi for their valuable suggestions, support throughout the course of the researches. I greatly appreciate to all the members of biochemistry laboratory and my friends who helped me a lot during the past five years.

I am grateful to Rotary Yoneyama Memorial Foundation for their support in the last one year.

Finally, yet importantly, I would like to express my heartfelt thanks to my beloved parents for their support and understanding all through these years.

REFEREES

This doctoral thesis was reviewed by the following members of Doctoral Dissertation Committee in Graduate School of Pharmaceutical Sciences of Chiba University.

Chief examiner: Professor Naoto Yamaguchi, Ph.D. (Pharm. Sci.), Graduate School of Pharmaceutical Sciences of Chiba University.

Assistant examiner: Professor Toshiharu Horie, Ph.D. (Pharm. Sci.), Graduate School of Pharmaceutical Sciences of Chiba University.

Assistant examiner: Professor Toshihiko Murayama, Ph.D. (Pharm. Sci.), Graduate School of Pharmaceutical Sciences of Chiba University.